UNIVERSITY OF TURIN

DOCTORAL SCHOOL IN LIFE AND HEALTH SCIENCES

PhD in Medical Pathophysiology – Cycle XXXIV

Horizontal tunnelling nanotube transfer to rescue dysfunctional mitochondria in diabetic nephropathy

Candidate:

Beatrice Corbetta

Tutor:

Prof.ssa Gabriella Gruden

INDEX

Abstract

Background. Diabetic nephropathy (DN) causes podocyte damage leading to the development of albuminuria. Mitochondrial dysfunction plays a key role in the pathogenesis of the podocyte injury in DN. Tunnelling nanotubes (TNTs) are a mechanism of communication among cells that allows intercellular transfer of subcellular organelles, including mitochondria. TNT formation occurs predominantly in response to stress and the cytosolic protein M-Sec plays a key role in the generation of TNTs. Mesenchymal stem cells (MSCs) are very efficient as mitochondrial donors as they highly express the mitochondrial Rho-GTPase Miro1 that drives the movement of mitochondria along TNTs. The aim of the present study was to establish whether a horizontal TNT-mediated transfer of mitochondria from MSCs to podocytes occurs in experimental diabetes and *in vitro* in podocytes exposed to diabetes-related insults and may have cytoprotective effects.

Methods. *In vitro study.* Podocytes exposed to either vehicle or diabetes-related insults (high glucose, glycated albumin, angiotensin-II, MCP-1) were co-cultured with MSCs. Experiments were also performed co-culturing podocytes with: 1) MSCs, 2) MSCs knockout for M-Sec; 3) MSCs pre-treated with rotenone to induce mitochondrial dysfunction; 4) MSCs obtained from non-diabetic/diabetic mice; and 5) MSCs overexpressing Miro1. TNT formation between podocytes and MSCs was assessed using the fluorescent plasma membrane dye WGA. Mitochondrial exchange was evaluated by monitoring mitochondrial transfer from MSCs carrying mitochondria-RFP to recipient podocytes stained with a cytoplasmatic fluorescent dye. Analyses were performed using both fluorescent and DIC microscopy. To explore the effect of mitochondrial transfer, we assessed podocyte apoptosis, expression of nephrin, Miro1, and mitochondrial genes (COX-1, ND4L), mitochondrial both membrane potential and oxidative stress by both fluorescence and real-time PCR. *In vivo study.* C57BL/6 mice were made diabetic (DM) with streptozotocin, while control non-diabetic animals (ND) were injected with vehicle. After eight weeks of diabetes, both DM and ND animals (n=5 per group) were injected with either buffer or MSCs (1.0×10^4 cells/g body weight once a week for 6 consecutive weeks) obtained from either WT (MSC^{WT}) or M-Sec KO (MSC^{KO}) mice. Injected MSCs carried mitochondria labelled with GFP. Animals were sacrificed after 14 weeks of diabetes. Urinary albumin was measured by enzyme-linked immunosorbent assay and creatinine by HPLC. Histological damage was assessed by PAS staining. Expression of slit-diaphragm proteins (nephrin and podocin), markers of fibrosis (fibronectin, collagen IV), inflammation (MAC-2, MCP-1, CCR2), mitochondrial transcription factor/genes (TFAM, COX-1, ND4L), and genes controlling mitochondrial biogenesis (PPARGC1A), fusion (MNF-1, OPA-1), fission (DNM1), and mitophagy (PINK1, PARK2) were analysed by immunofluorescence/immunohistochemistry and real time PCR.

Results. *In vitro study*. TNT formation occurs between MSCs and podocytes and was enhanced by exposure of podocytes to high glucose, glycated albumin, and MCP-1. Mitochondrial transfer was observed from MSCs to podocytes and was significantly augmented by exposure of podocytes to diabetes-related insults, while it was abolished by M-Sec silencing. Glycated albumin induced podocyte apoptosis, nephrin downregulation, and mitochondrial dysfunction. These effects were diminished/prevented when podocytes were co-culture with functional MSCs, while MSCs either lacking M-Sec or pre-treated with rotenone failed to rescue podocytes. MSCs from diabetic mice formed TNTs with podocytes; however mitochondrial transfer towards podocytes was significantly reduced. Expression of Miro1 was diminished in MSCs obtained from diabetic mice as well as in MSCs exposed to MCP-1 and glycated albumin. Miro1 overexpression in MSCs-DM not only re-established the efficiency of MSCs as mitochondrial donors, but also ameliorated mitochondrial parameters in recipient cells.

In vivo study. After 8 weeks of diabetes, levels of albuminuria were significantly greater in DM than ND mice, indicating the development of early DN. After 6 weeks of treatment with MSCs/vehicle, blood glucose and glycated haemoglobin were significantly higher and body weight significantly lower in DM compared to ND mice. In DM animals, treatment with either MSC^{WT} or MSC^{KO} did not affect these parameters. DM mice showed an over six-fold increase in albumin/creatinine ratio compared to controls. Diabetes-induced albuminuria, renal function decline, nephrin and podocin down-regulation, mitochondrial dysfunction, mesangial expansion and overexpression of extracellular matrix component were markedly reduced by treatment with MSC^{WT}, while treatment with MSC^{KO} was ineffective. By contrast, both MSC^{WT} and MSC^{KO} improved inflammation in diabetic mice. Importantly, GFP-labelled-mitochondria were observed in podocytes of DM mice injected with MSC^{WT}, while they were almost absent in DM mice treated with MSC^{KO}.

Conclusions. In conclusion, this study provides evidence that TNT-mediated exchange of mitochondria from MSCs to podocytes occurs both in vitro and *in vivo* in the context of diabetes and rescues diabetes-induced mitochondrial dysfunction and injury in podocytes, resulting in amelioration of the glomerular injury *in vivo*. The cytoprotective effect of MCSs obtained from DM mice was diminished because of reduced expression of Miro1 hampered mitochondrial transfer to podocytes via TNTs.

1. Introduction

1.1 Diabetic nephropathy

1.1.1 Epidemiology

There are 537 million people with diabetes worldwide and this number is expected to rise to 784 million by 2045 with a disproportionate increase in low-to middle-income countries[1]. The driving force behind the increasing prevalence of diabetes is the global pandemic of obesity. Diabetic nephropathy (DN) is a life-threatening microvascular complication of diabetes affecting ~30-40% of type 1 (T1DM) and type 2 (T2DM) diabetic patients[2]. DN is the leading cause of end-stage renal disease (ESRD), accounting for approximately 40% of new patients requiring renal replacement therapy[3]. Moreover, DN is an important risk factor of cardiovascular (CV) both morbidity and mortality and most people with DN die for CV diseases prior to ESRD development[1,4,5].

1.1.2. Clinical features

DN is characterised by both increased glomerular permeability to proteins and relentless decline in renal function. Albuminuria is both an early abnormality and a biomarker of DN. Albuminuria is classified as normoalbuminuria (< 20 μg/min), microalbuminuria (20-200 μg/min) and macroalbuminuria (> 200 μg/min)[6]. Diabetic patients undergo annual screening for early detection of albuminuria. Screening is usually performed by measuring the albumin-to-creatinine ratio (ACR) (normal <30 μg/mg, microalbuminuria 30-299 μg/mg, macroalbuminuria <300 μg/mg) in a morning urine sample. Two out of three positive tests performed over a period of 3-6 months are required to confirm the diagnosis. DN screening also includes the annual assessment of renal function by measurement of serum creatinine. Glomerular filtration rate (eGFR) is estimated using the Chronic Kidney Disease Epidemiology Collaboration (CDK-EPI, https://www.kidney.org/professionals/kdoqi/gfr) equation and stratified in 5 stages according to the National Kidney Foundation[7]. However, albuminuria is not always present and the non-albuminuric form of diabetic kidney disease (DKD) is the most prevalent variant of DKD, at least in T2DM patients[6,7,8]. Nevertheless, albuminuria still remains a major risk factor for progression[9].

1.1.3. Glomerular abnormalities

Glomerular abnormalities in DN comprise thickening of the glomerular basement membrane (GBM), expansion of the mesangial area, and podocyte dysfunction/damage[10]. Thickening of the GBM, resulting from overproduction of matrix components, reduced turnover, and diminished expression/activity of matrix metalloproteinases (MMPs)[11,12] precedes the development of

albuminuria and is a predictor of renal survival[13]. Excess mesangial cells deposition in the mesangium due to both increased production and reduced degradation of mesangial matrix components leads to mesangial expansion, ultimately resulting in glomerulosclerosis and profoundly affects renal function[14]. Podocytes are highly specialized glomerular epithelial cells that form the glomerular filtration barrier together with the fenestrated endothelium and the GBM[15,16]. Podocytes have a very complex structure. The podocyte cell body bulges into the urinary space and gives rise to long primary processes that branch into foot processes (FPs), enwrapping the glomerular capillaries[17]. FPs of neighbouring podocytes interdigitate, leaving between them filtration slits that are bridged by a junction, named slit diaphragm (SD). The transmembrane protein nephrin is a key component of the SD and mutation of nephrin causes the development of nephrotic syndrome[18]. Several podocyte abnormalities are observed in DN including loss of nephrin, foot process effacement, lower podocyte density, and absolute podocyte loss secondary to either podocyte apoptosis or detachment[19].

1.1.4 Pathogenesis

1.1.4.1 Hyperglycemia. Clinical intervention studies have convincingly proven that hyperglycemia is a key determinant in the onset/progression of DN[20,21,22.]. A large number of both *in vivo* and *in vitro* experiments have demonstrated that hyperglycemia causes both cell hypertrophy and enhanced deposition of extracellular matrix components in mesangial cells. Moreover, exposure of podocytes to high glucose (HG)/hyperglycemia induces nephrin loss, changes in the production/degradation of extracellular matrix components, enhanced Transforming Growth Factor Beta 1 (TGF-β1) signalling, remodelling of the actin cytoskeleton, downregulation of adhesion molecules, and podocyte apoptosis[23,24]. Glucose enters into glomerular cells via the Glut-1 and Glut-4 transporter. Excess glucose entry into cells increased flux through the polyol pathway, accumulation of advanced glycation end product (AGEs), activation of protein kinase C (PKC), and increased hexosamine pathway activity that are considered the predominant mechanisms of glucotoxicity in renal cells[25,26]. Moreover, binding of AGEs to the advanced glycation end product receptor (RAGE) expressed on both mesangial cells and podocytes also contributes to glomerular injury[27,28]. Finally, several cytokines such as TGF-β1, Connective Tissue Growth Factor (CTGF), Vascular Endothelial Growth Factor (VEGF), Insulin growth factor-1 (IGF-I), Angiotensin II (AT-II), and Monocyte Chemoattractant Protein-1 (MCP-1) are modulated by hyperglycemia and play a pivotal role in mediating the response of both podocytes and mesangial cells to HG/hyperglycemia by inducing sclerosis, inflammation, and enhanced permeability[25].

1.1.4.2 Hemodynamic insult. Convincing evidence indicates that an increased haemodynamic insult, secondary to elevations of both systemic and glomerular arterial pressure, in the setting of hyperglycaemia, is important in conferring susceptibility to kidney damage. In diabetes, glomerular hypertension is driven by an overactive renin-angiotensin-system (RAS), causing efferent arteriole vasoconstriction, and by enhanced proximal tubular glucose/sodium reabsorption, leading to de-activation of the tubular-glomerular feedback allowing afferent arteriolar vasodilation. *In vitro* studies have shown that mechanical stretch, mimicking glomerular capillary pressure, can enhance both TGF-β1 and extracellular molecule production in mesangial cells[29,30]. Moreover, exposure of podocytes to stretch induced cell hypertrophy[31] and reorganisation of the actin cytoskeleton[32], and integrin downregulation, leading diminishes podocyte adhesion to the GMB[33,34]. Importantly, podocyte stretching causes both nephrin downregulation and apoptosis through an autocrine mechanism mediated by AT-II[30,31]. Therefore, glomerular hypertension magnifies the deleterious effect of hyperglycemia on glomerular cells. Recently, glomerular capillary hypertension, induced by thrombus formation in the efferent arteriole, was shown to increase podocyte intracellular Ca^{2+} concentration in living mice, providing the first *in vivo* evidence that podocytes are mechanosensitive[35].

1.1.4.3 Oxidative stress. An excess of reactive oxygen species (ROS) plays an important role in the pathogenesis of DN[36]. Hyperglycemia-induced ROS accumulation cause oxidative stress that has several deleterious effects, including peroxidation of cell membrane lipids, DNA damage, protein modification, activation of both pro-inflammatory and pro-fibrotic pathways, and cell apoptosis[37]. The predominant source of ROS in renal cells is still a matter of debate; however, both mitochondria and NADPH oxidases (NOXs) are believed to be important[36,38]. The mitochondrial electron transport chain (ETC) is a potential source of mitochondrial ROS (mtROS) as electrons leaking from the ETC react with oxygen to form superoxide anions[39]. Accumulation of mtROS induces cardiolipin oxidation, leading to mitochondrial outer membrane permeabilization, cytochrome c release into the cytosol, and caspase-dependent apoptosis[40,41]. Moreover, mtROS can also trigger inflammation via activation of both the proinflammatory transcription factor Nuclear factor kappa B (NF-kB) and the inflammasome[42]. Enhanced mtROS production has been demonstrated in *db/db* mice by real-time mitochondrial redox assessment[43]. Moreover, there are reports showing amelioration of DN in animals treated with mitochondria-targeted antioxidants[44,45]. Among the seven isoforms of NOXs, both Nox4 and Nox5 expression are increased in the human diabetic kidney, as well as in glomerular cells exposed to HG, AGE, AT-II and TGF-β. Intervention studies in experimental diabetes have

shown that podocyte-specific Nox4 deletion ameliorates experimental DN[46] while podocyte-specific Nox5 expression causes podocyte damage and albuminuria[47].

1.1.4.4 Inflammation: The MCP-1-CCR2 system. There is growing evidence of an important role of inflammation in the pathogenesis/progression of DN. Glomerular monocyte infiltration occurs in both human and experimental DN. The chemokine monocyte chemoattractant protein-1 (MCP-1) is expressed by both resident glomerular cells and infiltrating monocytes and overexpressed in the diabetic glomeruli[48]. Several diabetes-related insults and mediators, such as HG, AT-II, AGEs, mechanical stretch, TGF-β1, and Tumor Necrosis Factor Alpha (TNF-α) are potent MCP-1-inducers in glomerular cells. MCP-1 can contribute to the onset and progression of DN by fuelling local inflammation through monocyte recruitment[49,50]. Indeed, activated monocyte/macrophages release ROS and both pro-inflammatory (Interleukin 1 Beta (IL-1β), TNF-α, Interferon Gamma (IFN-γ)) and pro-sclerotic (TGF-β1) cytokines, which in turn can enhances fibronectin production in mesangial cells and induce nephron downregulation in podocytes[51,52,53]. Furthermore, both mesangial cells and podocytes express CC chemokine receptor 2 (CCR2) and MCP-1 may contribute to the development of DN by directly inducing deleterious effects in resident glomerular cell. In mesangial cells MCP-1 enhances expression of both Intercellular Adhesion Molecule 1 (ICAM-1) and fibronectin and partially mediates HG-induced TGF-β1, fibronectin, and collagen type IV (C-IV) overproduction[54,55]. Moreover, in podocytes MCP-1 induces nephrin loss, apoptosis[52]. In mice, pharmacological agents blocking the MCP-1/CCR2 system ameliorate both functional and structural abnormalities of DN[56].

1.1.4.5 Mitochondrial dysfunction. Mitochondrial dysfunction plays an important role in the pathogenesis of DN[57]. Exposure of podocytes to high glucose reduces mitochondrial oxidative phosphorylation (OXPHOS)[58] and glomeruli from Pima Indians with early DN show dysregulation of genes encoding components of the respiratory chain[59]. Moreover, a recent study has shown that hyperglycemia induces Smad4 localization to mitochondria of podocytes, leading to a reduction in OXPHOS and an increase in ROS production[60]. Damaged mitochondria not only reduce ATP production, but also release dangerous molecules that can magnify injury. Excess generation of ROS can lead to oxidative stress and mitochondrial DNA (mtDNA) damage mitochondrial release of cytochrome c can trigger apoptosis, and release of free mtDNA can promote inflammation[61,62]. mtDNA is highly susceptible to oxidative stress because of lack of protective histone proteins and proximity to mROS. Accumulation of oxidative mtDNA lesions and loss of mtDNA copy number is observed in experimental DN[63,64] and HG reduces mtDNA copy number in podocytes[65]. Highly orchestrated processes of mitochondrial quality control (fission/fusion, biogenesis, mitophagy)

enable cells to avoid the dangers of mitochondrial injury. Mitochondrial fusion reduces mitochondrial stress by mixing the content of both damaged and healthy mitochondria, thus diluting stress[66]. Mitochondrial fission segregates damaged portions of the mitochondria that are then removed by mitophagy[67]. Finally, defective mitochondria can be replaced by through mitochondrial biogenesis[68]. These mechanisms of quality control are particularly important in cells exposed to stressful conditions and/or having enhanced metabolic needs as glomerular cells in diabetes. Enhanced mitochondrial fragmentation in podocytes has been reported in experimental models of DN and in kidney biopsy samples from patients with DN[69,70]. Moreover, podocyte-specific deletion of the dynamin-related protein 1 (Drp1), which plays a key role in *fission*, blocked mitochondrial fragmentation, improved mitochondrial fitness and protected against DN progression in mice[71].

Mitophagy is predominantly mediated by the PTEN-induced kinase 1 (PINK1)/Parkin pathway that leads to mitochondrial tagging and delivery to the autophagosomes[72]. Increasing evidence indicates an impairment of mitophagy in DN. PINK1 expression is reduced in diabetic mice and in cultured podocytes exposed to HG[73] likely via downregulation of the SIRT1-PGC1α-FOXO1 pathway[74,75].

Mitochondrial biogenesis. PGC-1α is the master regulator of mitochondrial biogenesis and PGC-1α silencing leads to podocyte injury. Studies in both humans and experimental animals have shown that glomerular PGC-1α expression is reduced in DN[76, 77].

1.2 Tunneling nanotubes (TNTs)

1.2.1 TNT Morphology

Tunneling nanotubes (TNTs) are a novel mechanism of cell-to-cell communication. TNTs are straight open-ended membrane channels that connect cells over long distances. They are typically 50 to 700 nm in diameter with lengths up to several cell diameters and contain a F-actin backbone. However, in some types of cells they can also have a microtube backbone with an increased diameter and a prolonged lifetime[78]. As characteristic properties, TNTs lack contact to the substratum and this distinguishes them from filopodia. Unlike classical membrane extensions, TNTs were shown to mediate membrane continuity between interconnected cells[79]. TNTs have been demonstrated in a variety of cell types *in vitro*, including monocytes/macrophages[80,81], immune[82,83,84,85], endothelial[86], cancer[87], stem cells[88]. TNTs are very sensitive to light, mechanical stresses, and chemical fixation making it difficult to identify and visualize TNTs in living tissues. Despite these technical issues, recent studies succeeded in the identification of TNT-like structures both *in vivo* and *in situ*[89,90,91,92]. Alarcon-Martinez *et al.* demonstrated TNTs interconnecting pericytes in the mouse retina[93]. Desir *et al*. visualized TNTs *in vivo* in human pancreatic cancer specimens by multiphoton fluorescence microscopy[94]. Finally, Osswald *et al.* observed TNTs in an animal model of malignant brain tumor *in vivo*[95].

1.2.2 TNT formation and M-Sec

M-Sec, a cytoplasmic protein of 73 kDa, is a central factor in the induction of plasma membrane protrusion during TNT formation in several cell types. M-Sec also known as TNFα-induced protein 2 (TNFAIP2) or B94, was originally identified as a TNF-α-inducible gene in umbilical vein endothelial cells (HUVEC), but also IL-1β and lipopolysaccharide (LPS) can induce M-Sec mRNA expression[96,97]. M-Sec mRNA and protein have is enriched in lymphoid tissues. Moreover, M-Sec is highly expressed in myeloid lineages of both mouse and human origin, including dendritic cells, mononuclear progenitor cells, mature peripheral monocytes and macrophages[82,96]. M-Sec is crucial for TNT formation in Raw264.7 macrophages and M-Sec downregulation greatly reduces TNT formation in this cell type. Moreover, ectopic expression of M-Sec in HeLa cells induces formation of TNTs[98]. M-Sec facilitates TNT outgrowth by promoting cytoskeletal remodelling. Specifically M-Sec initiates actin polymerization, then elongation of actin polymers is controlled by member of the Rho protein family (Cdc42, Rac1 and RhoA20)[99] and in particular by the Ras-like small GTPase RalA[98, 100,101].

1.2.3 Functional role of TNT

TNT form *de novo* predominantly from cells exposed to stresses including serum starvation, hypoxia, inflammation and oxidative stress, suggesting that TNTs may serve as a survival mechanism[102]. However, TNTs are also involved in physiological processes, such as osteoclast differentiation[103], electrical coupling and calcium signaling[104], embryonic development[105] and maintenance of homeostasis. The mechanisms for TNT direction guidance have not been clarified yet, however, in astrocytes both the calcium binding protein S100A4 and the RAGE receptor have been implicated in TNT guidance[106]. TNTs mediate the exchange of various factors, such as ions, nucleic acids, and proteins between interconnected cells[102]. TNT-mediated calcium signalling contributes to communication between neurons[104]. Moreover, dendritic cells use TNTs for intercellular exchange of antigens[87]. At variance with other intercellular communication systems TNTs also allow exchange of organelles, including lysosomes and mitochondria[107,108,109]. Mitochondria have been observed in TNTs connecting many different cells types[110] including renal proximal tubular epithelial cells (RPTEC)[111], astrocytes[112], endothelial cells[113,114], neuronal cells[112,115] and monocyte-derived macrophages[116]. Of interest, TNTs can also mediate an uni/bidirectional exchange between progenitor/stem and differentiated cells. TNT-mediated transfer of mitochondria from both vascular smooth muscle cells and renal tubular cells to progenitor cells induces proliferation/differentiation of progenitor cells[117,111]. Mitochondrial transfer in the opposite direction has been shown to improve survival of stressed HUVEC and to reprogram cardiomyocytes back to a progenitor-like state, possibly representing a regenerative mechanism leading to selective survival/proliferative advantages[118,86].

On the other hand, TNTs may also be deleterious. Viruses/prions can “hijack” TNTs for cell to cell spreading[119,120]. Moreover, in neurodegenerative diseases, TNTs increase target cells vulnerability by favouring the rapid transfer of amyloid and tau peptides[121]. Finally, an increasing number of studies have proven a deleterious role of TNTs in cancer. Indeed, malignant cells take advantage of TNTs to drive tumors both formation and progression[91], and to acquire chemoresistance[122].

1.2.4 Evidence of M-Sec-TNT system in the kidney

We are recently proven that podocytes exposed to injury can form TNTs via an M-Sec dependent mechanism[123]. In cultured stressed podocytes, M-Sec deletion abolished TNT-mediated mitochondria transfer and altered mitochondrial bioenergetics. Re-expression of M-Sec re-established TNT formation and mitochondria exchange, rescued mitochondrial function, and partially reverted adriamycin-induced podocyte injury. In *Balb/c* mice, M-Sec deletion caused podocyte injury, mitochondrial abnormalities, and spontaneous development of progressive focal segmental

glomerulosclerosis (FSGS). Moreover, there was a compensatory M-Sec overexpression in podocytes in both human and experimental FSGS. Transfer of organelles from healthy to damaged podocytes via TNTs may represent an important survival mechanism and TNT-mediated mitochondrial transfer is now included among the mechanisms of mitochondrial quality control.

1.3 Mesenchymal stem cells (MSCs)

1.3.1 MSC properties

Mesenchymal stem cells (MSCs) are characterized by their multilineage differentiation capacity, notably into osteocytes, adipocytes, and chondrocytes[124]. They also express specific cell surface markers that include CD105 (endoglin), CD44, CD49f, SCA-1, CD73, CD90, CD19, but no CD79, CD14, CD11b and the hematopoietic markers CD45[125,126].

Beside the bone marrow, MSCs have been isolated from other tissues including the human placenta[127], umbilical cord[128] and adipose tissue-derived mesenchymal stem cells (AT-MSCs)[129, 126].

1.3.2 Bone Marrow (BM)-MSCs and DN

In the last decade, intervention studies in animal models of DN have proven the therapeutic potential of MSCs obtained from different sources, including bone marrow (BM-MSCs). Administration of BM-MSCs via the renal artery decreased urinary albuminuria and improved renal function in streptozotocin (STZ)-induced diabetic rats with established DN. This effect was paralleled by amelioration of diabetes-induced podocyte loss, foot processes effacement, and downregulation of podocyte protein[130]. In a similar experimental model, intravenous infusion of BM-MSCs also reverted glomerulosclerosis, extracellular matrix (ECM) deposition, and diminished macrophage infiltration and inflammation[131]. More recently, a study performed on type 1 diabetic mice has shown that BM-MSCs limit inflammation-related injury through the phenotypic switch of macrophage from a pro-inflammatory (M1) to anti-inflammatory (M2) phenotype[132]. Emerging evidence shows that the efficacy of MSCs in ameliorating DN is mainly due to MSC release of soluble factors and extracellular vesicles (EVs)[133]. In line with this, Nagaishi *et al*. demonstrated that the beneficial effect of BM-MSCs on renal damage, macrophage infiltration, interstitial fibrosis, and glomerular injury in experimental DN was reproduced by treatment with MSC conditioned media[134]. Moreover, LV *et al.* showed that conditioned media from BM-MSC inhibited the TGF-β/Smad prosclerotic pathway in mesangial cells exposed to a HG milieu. This beneficial effect was abolished by treatment with an antibody direct against bone morphogenetic protein-7 (BMP-7). This suggest that BMP-7 secreted by MSCs was involved[135]. Besides soluble factors, EVs both exosomes (Exos) and microvesicles (MVs), may also mimic the effect of their parent cells via horizontal transfer of functional microRNAs (miRNAs), mRNAs, and proteins to target cells. Several studies have shown that treatment with MSC-EVs is safe and has renoprotective effects in models of DN. In diabetic animals, treatment with BM-MSC-Exos abolished apoptosis and tubular epithelial cells (TEC) damage, improved renal function, and reduced renal fibrosis by acting on the mTOR signalling pathway and autophagy[136].

Similarly, BM-MSC-EVs administered in a therapeutic-like regimen inhibit the progression of the functional and morphological dysfunction caused by DN[137].

1.3.3 MSCs and TNT-mediated mitochondrial transfer

An increasing body of preclinical studies showed that MSCs are particularly efficient as mitochondrial donors to stressed cells and TNT-mediated mitochondrial transfer is one of the mechanisms used by MSCs to repair tissue damage and to promote tissue regeneration. The particular efficiency of MSCs in shuttling mitochondria along TNTs has been attributed to their high expression levels of Miro1, a calcium-sensitive mitochondrial Rho-GTPase that is responsible for mitochondrial association with the microtubule mobility complex and drives the movement of mitochondria along TNTs[138,139]. In an *in vitro* ischemia/reperfusion model, Liu *et al.* showed that the transfer of functional mitochondria from BM-MSCs through TNTs rescued HUVEC from oxygen and nutrients deprivation-induced apoptosis[140] and a similar anti-apoptotic effect was observed in cardiomyocytes exposed to oxidative stress[141]. Babenko *et al.* reported that transfer of healthy mitochondria from BM-MSCs via TNTs rescued the bioenergetics of cultured astrocytes and neuron-like PC12 pheochromocytoma cells from oxygen–glucose deprivation-induced oxidative stress and mitochondrial damage, respectively[115]. Furthermore, *in vivo* treatment with BM-MSCs improved the neurological impairments of cerebral ischemic rats and this effect was further ameliorated by administration of BM-MSCs overexpressing Miro1. Notably, this study showed that mitochondria transfer could even rescue mitochondrial respiration in mitochondrial-depleted cells[115]. Islam *et al.* demonstrated that the mitochondrial transfer via TNTs from MSCs to pulmonary alveolar epithelial cells has protective effects in a murine model of LPS-induced acute lung injury[108]. Finally, Ahmad *et al.* reported the protective effect of BM-MSCs in an *in vivo* asthma models of rotenone-induced airway epithelial injury and allergic airway inflammation and, *in vitro*, in bronchial epithelial cells treated with conditioned medium derived from macrophages exposed to interleukin-13 (IL-13)[138]. Overall, these studies demonstrated that the ability to replace dysfunctional organelles via TNTs is an important survival mechanism and is of particular relevance in terminally differentiated cells.

2. Aim of the study

DN is a microvascular complication of diabetes mellitus (DM) characterized by increased glomerular permeability to proteins. Current therapeutic strategies for the treatment of DN are effective; however, DN is still a major cause of end stage renal failure (ESRF) in the Western world. Mitochondrial dysfunction plays a key role in the pathogenesis of the glomerular damage in DM and hyperglycemia-induced mitochondrial oxidative stress can cause mutations of mtDNA. Podocytes are responsible for maintaining the perm-selectivity of the glomerular filtration barrier. As podocytes are terminally differentiated cells, mtDNA mutations can accumulate in these cells and lead to permanent alterations in mitochondrial bioenergetics. TNTs are straight open-ended membrane channels that connect cells over long distances. They lack contact to the substratum and can mediate the intercellular transfer of small subcellular organelles, including mitochondria. They form predominantly from stressed cells via activation/expression of Akt, phosphoinositide 3-kinase (PI3K), p53, mTOR, and M-Sec. TNTs may represent a mechanism for the replacement of dysfunctional mitochondria, but their relevance in DN is unknown. MSCs are very efficient mitochondrial donors. The underlying mechanism is unknown; however, elevated Miro1 expression may play a role as Miro1 is responsible for mitochondrial association with the microtubule mobility complex and drives the movement of mitochondria along TNTs.

The general purpose of the present project was to explore the potential relevance of a mitochondrial transfer from donor MSCs to the recipient podocytes via TNTs, both *in vitro* and *in vivo*, and investigate if this transfer can ameliorate DN.

3. Research design and Methods

3.1 *In vitro* study

3.1.1 Cells

Conditionally immortalised human podocytes (kindly provided by Prof. Saleem) were cultured and expanded at 33°C, 5% CO2, in RPMI medium, containing 10% fetal bovine serum (FBS), 100U/mL of penicillin/streptomycin, 2mM L-glutamine, insulin, transferrin and sodium selenite. Subsequent experiments were performed using podocytes differentiated at 37°C for 15 days.

Primary murine podocytes were isolated from mice at 4 weeks of age. Mice were anesthetized and perfused with a HBSS solution containing $8x10^7$ surface inactivated beads (Dynabeads, Invitrogen). Decapsulated kidneys were diced and digested in a collagenase A (1 mg/ml) solution for 30 minutes at 37 °C and then passed through a 100 μm (Falcon; BD Biosciences) mesh. Glomeruli were isolated using a magnetic particle concentrator and then repeatedly washed to remove tubules and then plated on collagen type IV-coated dishes at 37°C in DMEM medium with 10% FBS, 100 U/ml penicillin/streptomycin, 100 mM HEPES, 1 mM sodium bicarbonate, and 1 mM sodium pyruvate. Subculture of primary podocytes was performed by detaching the glomerular cells with 0.25% trypsin-EDTA, followed by sieving through a 40 μm cell strainer (Falcon; BD Biosciences), and plating on collagen type IV-coated dishes. Cells were used before the third passage in all experiments.

Human mesenchymal stem cells (hMSCs) were purchased from Lonza (Basel, Switzerland) and cultured in mesenchymal stem cell basal medium (MSCBM, Lonza) with mesenchymal stem cell growth supplement (MCGS, Lonza), 100U/mL of penicillin/streptomycin, 2mM L-glutamine and GA-1000. Cells were used for experiments until the sixth passage.

Murine bone marrow (BM) mesenchymal stem cells (BM-MSCs) were isolated from wild type (WT), M-Sec knock-out (KO), non diabetic (ND) and diabetic (DM) mice. Bone marrow (BM) cells were flushed from tibial and femoral cavities under sterile conditions and plated at 37°C in hypoxic conditions (5% O2 and 10% CO2) for 7-10 days in MesenCult™ Expansion Medium with MesenPure™, 100U/mL of penicillin/streptomycin and 2mM L-glutamine. Cells were subcultured until passage three and then characterized. Flow cytometry was performed to analyse the phenotypic properties of BM-MSCs using the following markers: FITC-CD44, FITC-SCA-1, FITC-CD49f, PE-CD45. Oil Red O staining was performed to assess the ability of MSCs to differentiate in adipocytes.

3.1.2 Diabetes-related insults

Conditionally immortalized human podocytes were exposed to either glycated albumin (GA, 100 µg/ml) for 72 hours, or MCP-1 (10 ng/ml) for 24 hours, or Angiotensin II (AT-II, 1µM) for 24 hours or high glucose concentrations (HG, [glucose]=30mM) for 72 hours. Cells exposed to normal glucose concentrations (NG= 10 mM made iso-osmolar with mannitol) or vehicle were used as controls. In a subset of experiments, podocytes were exposed to either rotenone (10 nM) for 2 hours or Latrunculin-B (200 nM) for 1 hour to induce mitochondrial dysfunction and inhibit TNT formation, respectively.

3.1.3 M-Sec Sh-RNA

hMSCs were transfected using Lipofectamine 3000 Transfection Reagent (Thermo Fisher Scientific) with a plasmid construct encoding m-Sec-specific sh-RNA (shRNA: 5'-GATCCGACTGCTGGAGGCCACATTCCTGT-3', scramble negative control: 5'-GCACTACCAGAGCTAACTCAGATAGTACT-3') cloned in a pGFP-V-RS vector (ExactHuSH, OriGene Technologies Inc). Knockdown efficiency was confirmed by western blot analysis.

3.1.4 Miro1 overexpression

BM-MSCs were transfected with a human adenovirus (Vector Biolabs, Malvern, PA) encoding Miro1 (98% homologous to the human gene) and the reporter protein Green Fluorescent Protein (GFP) (Ad-Miro1), with a standardised multiplicity of infection (MOI) of 200. Empty vector (Ad-Mock) was used as a control for transduction. Experiments were performed 6 hours after adenoviral transduction at 37C°.

3.1.5 TNTs

Podocytes, exposed to diabetes-related insults, were stained with a cytoplasmic dye (CellTracker Blue) and co-cultured with MSCs. To visualize plasma membrane and TNTs, cells were stained with 5 µg/ml of wheat germ agglutinin (WGA) conjugated with Alexa Fluor®-488 (Thermo Fisher Scientific) in HBSS for 10 minutes at 37°C and analysed with a Zeiss Apotome II Microscope controlled by Axiovision software. The number of podocytes connected with MSCs by straight WGA-labelled structures that did not adhere to the substrate, as assessed by Z-stack, and with diameter smaller than 1 µm was counted in blind and results expressed as percentage of total counted cells (at least 150 cells). To visualize TNT either actin or tubulin-based backbone, cells were fixed with 4% PFA for 30 minutes, incubated with 3% BSA in PBS for 30 minutes for blocking the non-specific binding sites and then incubated with Phalloidin-FITC or mouse anti-alpha-tubulin-FITC for 1 hour at 37°C.

3.1.6 Mitochondrial transfer

Podocyte pre-exposed to diabetes-related insults were stained with Cell-Tracker Blue/Green and co-cultured with MSCs transfected with BacMam expression vector encoding a fusion of a fluorescent protein (RFP) with a specific mitochondrial protein (E1α pyruvate dehydrogenase) at 37°C. After 24h, co-cultures were analysed by live both fluorescence and differential interference contrast (DIC) microscopy. The percentage of podocytes containing RFP-labelled mitochondria was used as an index for the mitochondria transfer efficiency from donor cells to recipient cells. To control for TNT-independent transfer, experiments were performed using a 2 well ibidi culture-insert, where the two cell populations were separately seeded but shared the same culture medium. After cell attachment, the insert was removed (0.5 µm cell free gap) and the two populations co-cultured for 24 hours under gentle shaking. In a subset of experiments, to inhibit TNT formation, cells were treated with latrunculin-B (200 nM), an actin depolymerisation agent. Rotenone (50 nM) was used as positive control to induce mitochondrial dysfunction.

3.1.7 Mitochondrial Parameters

Mitochondrial membrane potential (MMP) was assessed by using JC-1 (1µg/ml, Thermo Fisher Scientific) for 15 minutes at 37°C. Mitochondrial superoxide production was measured by using Mitosox (3µM, Thermo Fisher Scientific) in HBSS for 10 minutes at 37˚C. Results were expressed as the percentage of fluorescence intensity per cell area (recipient cells).

3.1.8 Apoptosis

Apoptotic cells were detected in co-cultures by transferase-mediated dUTP nick end-labeling (TUNEL) assay (ApopTag® Red In Situ Apoptosis Detection Kit). Results were expressed as the percentage of positive recipient podocytes.

3.2 Animal study

3.2.1 Animals

Male C57BL/6 mice from Charles River Laboratories Italia were housed at a constant temperature and humidity with a 12-hour light/dark cycle and given free access to food and water. Both housing and care of laboratory animals were in accordance with Italian law (D.Lgs. 26/2014). All experimental protocols and studies were approved by the Ethical Committee of the University of Turin.

3.2.2 Streptozotocin-induced diabetes

8-week-old male C57BL/6 mice were made diabetic (DM) by intraperitoneal injection of STZ dissolved in citrate buffer (pH 4,5), (55mg/kg body weight/day) delivered in 5 consecutive days. Non-diabetic animals (ND) were treated with a citrate buffer alone. Diabetes onset was confirmed by blood glucose ≥ 250mg/dl 4 weeks later after the first injection of STZ.

3.2.3 Experimental protocols

After eight weeks of diabetes, both DM mice with established albuminuria and ND animals (*n*=5 per group) were injected (once a week for 6 consecutive weeks) with either vehicle or mitochondria-GFP-tagged MSCs (1.0×10^4 cells/g body/weight) obtained from either WT (MSC^{WT}) or M-Sec KO (MSC^{KO}) mice kindly provided by Prof. Ohno H (Riken, Japan). After 14 weeks of diabetes, animals were anesthetized and killed by decapitation. Kidneys were rapidly dissected, weighed and processed for subsequent analyses. A kidney was frozen in liquid nitrogen and stored at -80°C for mRNA and protein analysis. Half of the second kidney was formalin-fixed and paraffin-embedded for light microscopy; the remaining tissue was embedded in optimal cutting temperature (OCT) compound and snap-frozen in liquid nitrogen.

3.2.4 Metabolic and physiological parameters

Before sacrifice, blood samples were taken via saphenous vein puncture on alert 4-hours–fasted animals, and glucose levels were measured using a glucometer (Accu-chek; Roche). Glycated haemoglobin was assessed by quantitative immunoturbidimetric latex determination (Sentinel Diagnostic). Systolic blood pressure (SBP) was performed by tail-cuff plethysmography. Urine was collected over 18-hours, with each mouse individually housed in a metabolic cage and provided with food and water *ad libitum*. Urinary albumin concentration was measured by ELISA (enzyme-linked immunosorbent assay) Kit (Bethyl Laboratories), as either albumin excretion rate (AER, μg/18 hour) or albumin-to-creatinine ratio (ACR, μg/mg). Creatinine clearance was estimated from serum and urine creatinine concentrations, as determined by high-performance liquid chromatography (HPLC) according to the Animal Models of Diabetic Complications Consortium (AMDCC) guidelines.

3.3 Microscopy

Light Microscopy. Paraffin-embedded renal sections were stained using Periodic acid–Schiff (PAS). Mesangial area was analysed (percentage of glomerular area) from digital pictures of 15–20 glomeruli per kidney per animal using the Axiovision 4.7 software.

Fluorescent and DIC microscopy. A Zeiss APOTOME 2 system equipped with an incubator for live cell imaging/time-lapse microscopy and Nomarski optics for differential interference contrast (DIC) microscopy was used in the TNT study. DIC microscopy was utilized to avoid TNT phototoxic damage, sequences of optical planes (Z-stack) were acquired for reconstruction in the x-z plane.

3.4 mRNA analysis

Total RNA was extracted and purified from either the renal cortex or cells using TRIzol reagent (Thermo Fisher Scientific). After the quantification, one or two µg of total RNA underwent reverse transcription into cDNA using the High-Capacity Reverse Transcription kit (Thermo Fisher Scientific). Expression of Miro1 (Mm01304158), nephrin (Mm00497828), podocin (Mm00499929), fibronectin (Mm01256744), collagen type IV A1 (Mm00802377), MCP-1 (Mm00441242), CCR2 (Mm01216173), TFAM (Mm00447485), COX1 (Mm04225243, Hs02596864), ND4L (Mm04225306; Hs02596876), PINK1 (Mm00550827), PARK2 (Mm01323528), OPA1 (Mm00453879), DNM1L (Mm01342903), MFN1 (Mm00612599), PPARGC1A (Mm01208835) was quantitatively analysed by real-time PCR using pre-developed TaqMan reagents (Thermo Fisher Scientific). Relative expression was calculated using the comparative Ct method ($2^{-\Delta\Delta Ct}$). Results were normalized to the expression of appropriate housekeeping genes: HPRT, WT-1, GAPDH.

3.5 Protein analysis

Immunohistochemistry was performed in 4 µm-paraffin kidney sections of formalin-fixed tissue. After antigen retrieval in a citrate buffer (0.01M, pH=6.0), sections were exposed to 3% H_2O_2 to neutralize endogenous peroxidase activity and endogenous avidin-binding sites were blocked by incubation with 0.1% avidin and 0.01% biotin. Slides were then incubated with 3% bovine serum albumin (BSA) in PBS for 30 minutes for blocking the non-specific binding sites. Sections were then incubated overnight at 4°C with a rat anti-MAC2 (Cederlane) primary antibody. After washing with PBS, sections were exposed to a secondary biotinylated-labelled goat anti-rat antibody (Jackson Immuno Research Laboratories) for 1 hour, followed by incubation with horseradish peroxidase (HRP)-conjugated streptavidin (DAKO) for 1 hour and mounted. 3,3'- diaminobenzidine (DAB) was used as a chromogen substrate for HRP. A negative control was included in which the primary antibody was preincubated with a control peptide. Sections were visualized with an Olympus-BX4I microscope and digitized with a high-resolution camera (Carl Zeiss). On average 30 randomly selected glomeruli were assessed per mouse. Results were expressed either as the number of positive cells/glomerular area or as percentage area of positive staining per glomerulus.

Immunofluorescence. Snap-frozen kidney sections (3 µm) were fixed in cold acetone for 5 minutes and blocked in 3% BSA in PBS. Slides were then incubated overnight at 4°C with guinea pig anti-

nephrin (Progen Biotechnik), rabbit anti-podocin (Sigma-Aldrich), rabbit anti-fibronectin (Sigma-Aldrich) primary antibodies. After washing with PBS, fluorescein isothiocyanate-conjugated (FITC) swine anti rabbit (DAKO), Alexa Fluor 568 goat anti guinea pig (Thermo Fisher Scientific) secondary antibodies were added for 1 hour. After the incubation, sections were mounted and then examined using a APOTOME 2 microscope (Carl Zeiss). On average 30 randomly selected glomeruli were assessed per mouse. Results were expressed as the percentage area of positive staining per glomerulus.

Double immunofluorescence. Snap frozen kidney sections were fixed in cold acetone for 5 minutes and blocked with avidin-biotin solutions and 3% BSA in PBS for 30 minutes and then incubated overnight at 4°C with a primary antibody made in rabbit and directed against GFP (thermo fisher Scientific). After washing with PBS, sections were incubated with a swine anti-rabbit biotinylated (DAKO) for 1 hour and then streptavidin-FITC (DAKO) was added for 1 hour. After further blocking in 3% BSA, sections were incubated with a primary antibody against nephrin overnight at 4°C, followed by incubation with an Alexa Fluor 568 goat-anti guinea pig secondary antibody for 1 hour. Digitalized images were colour-combined and assembled into photomontages by using Adobe Photoshop (Universal Imaging Corporation, West Chester, PA).

3.6 Statistical Analysis

Data were expressed as means ± SEM, geometric mean (25th-75th percentile), and fold change over control. Non-normally distributed variables were log-transformed prior to the analyses. Data were analysed by the Student's t test or ANOVA, as appropriate. Least significant difference test was used for post-hoc comparisons. Values of $P<0.05$ were considered statistically significant.

4. Results

In vitro study

4.1 TNTs form between MSCs and podocytes exposed to diabetes-related insults

To assess whether TNTs form between podocytes and MSCs and if diabetes-related insults affect TNT formation, conditionally immortalized human podocytes were exposed to vehicle, serum deprivation, which is a well-known TNT inducer, or diabetes-related insults (HG, GA, AT-II, MCP-1). Cells were stained with the cytoplasmic dye CellTracker Blue and then co-cultured with human MSCs. After 24 hours, co-cultures were stained with Alexa Fluor®488-conjugated WGA (5µg/ml), which allows to visualize TNTs. Bridge-like structures interconnecting MSCs and podocytes were observed by both DIC and live fluorescence microscopy. These structures displayed the specific features of TNTs: they were straight, exhibited a width of less than 0.5 µm and a length of over several cell diameters (Figure 1). As assessed by Z-stack reconstruction, they did not adhere to the substrate, a feature that is specific to TNTs (Figure 1B,C). Following fixation, the identity of podocytes was confirmed by nephrin immunostaining (Figure 1D). TNTs interconnecting MSCs and podocytes had either an actin or a tubulin backbone (Figure 1E,F). Importantly, the number of podocytes connected to MSCs via TNTs was significantly enhanced in podocytes exposed to serum deprivation, HG, GA, and MCP-1 (Figure 1G), confirming the hypothesis that diabetes-related insults induce TNT formation. Notably, formation of TNTs, interconnecting MSCs and podocytes, was almost abolished by M-Sec silencing (Figure 1H), confirming the key role of M-Sec in TNT formation.

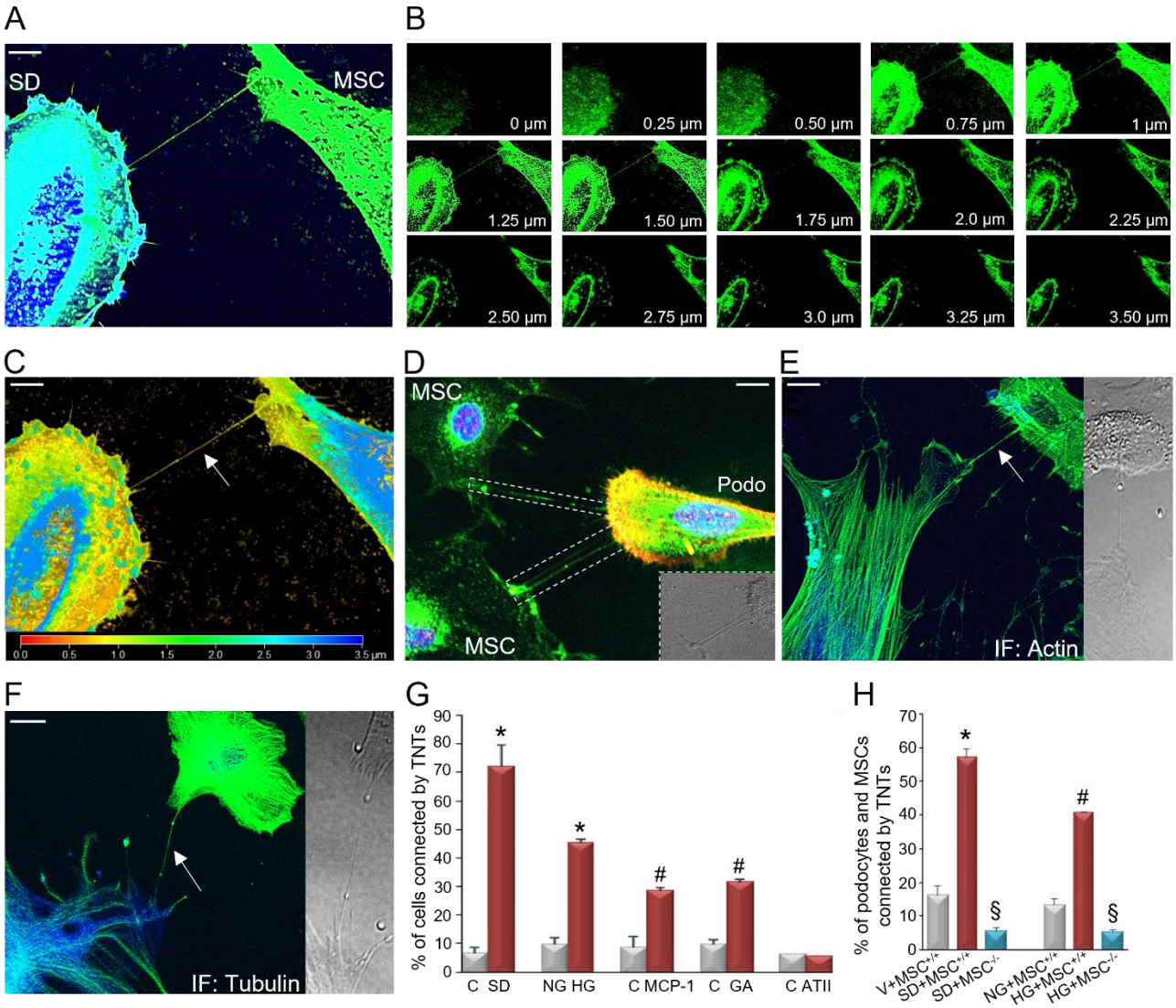

Figure 1. TNT-like channels form between MSCs and podocytes pre-exposed to diabetes related insults. Podocytes exposed to HG (25mM, 48h) were stained with the CellTracker Blue and co-cultured with MSCs. After 24 hours, co-cultures were stained with WGA-Alexa Fluor 488 to reveal TNTs. **(A)** A representative image showing a TNT-like channel, interconnecting a podocyte and a MSC is shown (magnification X630, bar=50µm). **(B)** Serial Z-stack images, acquired with a step-size of 0.25 µm, proved that TNTs did not adhere to the substrate. Colours in panel **(C)** represent the Z-depth (depth-coding; red: bottom, blue: top). **(D)** Podocyte and MSC co-cultures were stained with WGA-Alexa Fluor 488 to reveal TNTs. Then cells were fixed and stained for nephrin (RFP) to confirm podocytes identity (yellow merge) (magnification X630, bar=50µm). **(E, F)** Fluorescent staining for F-actin (Alexa Fluor 488-labeled phalloidin) and tubulin showed that TNTs bridging podocytes and MSCs (blue) contain either actin or tubulin (DIC image in the insert) (magnification X630, bar=50µm). **(G)** Podocytes were exposed to HG (25 mM, 48h), GA (100 µg/ml, 72h), AT-II (1 µM, 24h), or MCP-1 (10 ng/ml, 24h), labelled with CellTracker Blue and then co-cultured with MSCs. Co-cultures with podocytes pre-exposed to either vehicle or medium made iso-osmolar with mannitol (control [glucose]=10mM, NG) were used as controls. The percentage of podocytes and MSCs connected by TNTs is reported in the graph (n=3, *$p<0.001$* HG vs. NG; *#$p<0.01$* MCP-1 and GA vs. control). **(H)** Podocytes were exposed to either serum deprivation (SD 0.1%) or HG, stained with CellTracker Blue and then co-cultured with MSCs. After 24 hours, co-cultures were stained with WGA-Alexa Fluor 488 and analysed by fluorescent live cell microscopy to reveal TNTs. Experiments were performed using MSCs transfected with either M-Sec shRNA ($^{-/-}$) or a mock plasmid ($^{+/+}$). The percentage of podocytes and MSCs connected by TNTs is reported in the graphs (n=3, *$p<0.001$; #$p<0.01$* SD+MSC$^{+/+}$ and HG+MSC$^{+/+}$ vs. vehicle/NG; §$p<0.05$ SD+MSC$^{-/-}$ and HG+MSC$^{-/-}$ vs. vehicle/NG).

4.2 Mitochondrial transfer occurs between MSCs and podocytes via a TNT-M-Sec dependent mechanism

To test if TNTs interconnecting podocytes and MSCs were functionally active and allowed mitochondria transfer, conditionally immortalized human recipient podocytes were exposed to HG, GA, and MCP-1, labelled with CellTracker Green/Blue, and then co-cultured with donor MSCs, carrying RFP-labelled mitochondria. Rotenone was used as positive control. After 24 hours of co-cultures, fluorescent mitochondria were seen along TNTs and in the cytosol of recipient podocytes, indicating mitochondrial transfer (Figure 2A-D). Quantification showed that TNT-mediated mitochondrial transfer was significantly enhanced by podocyte exposure to either rotenone or diabetes-related insults. Mitochondrial transfer was almost abolished when M-Sec was silenced in donor MSCs (Figure 2E). Moreover, no transfer was observed when cells were either seeded in µ-slide 2 well co-culture that prevents direct cell-to-cell contact or treated with the actin depolymerizing agent latrunculin-B (Figure 2F,G). Collectively, these data indicate that M-Sec-dependent-TNT-mediated mitochondrial trafficking occurs from MSCs to podocytes and is enhanced towards podocytes that are exposed to insults inducing mitochondrial dysfunction.

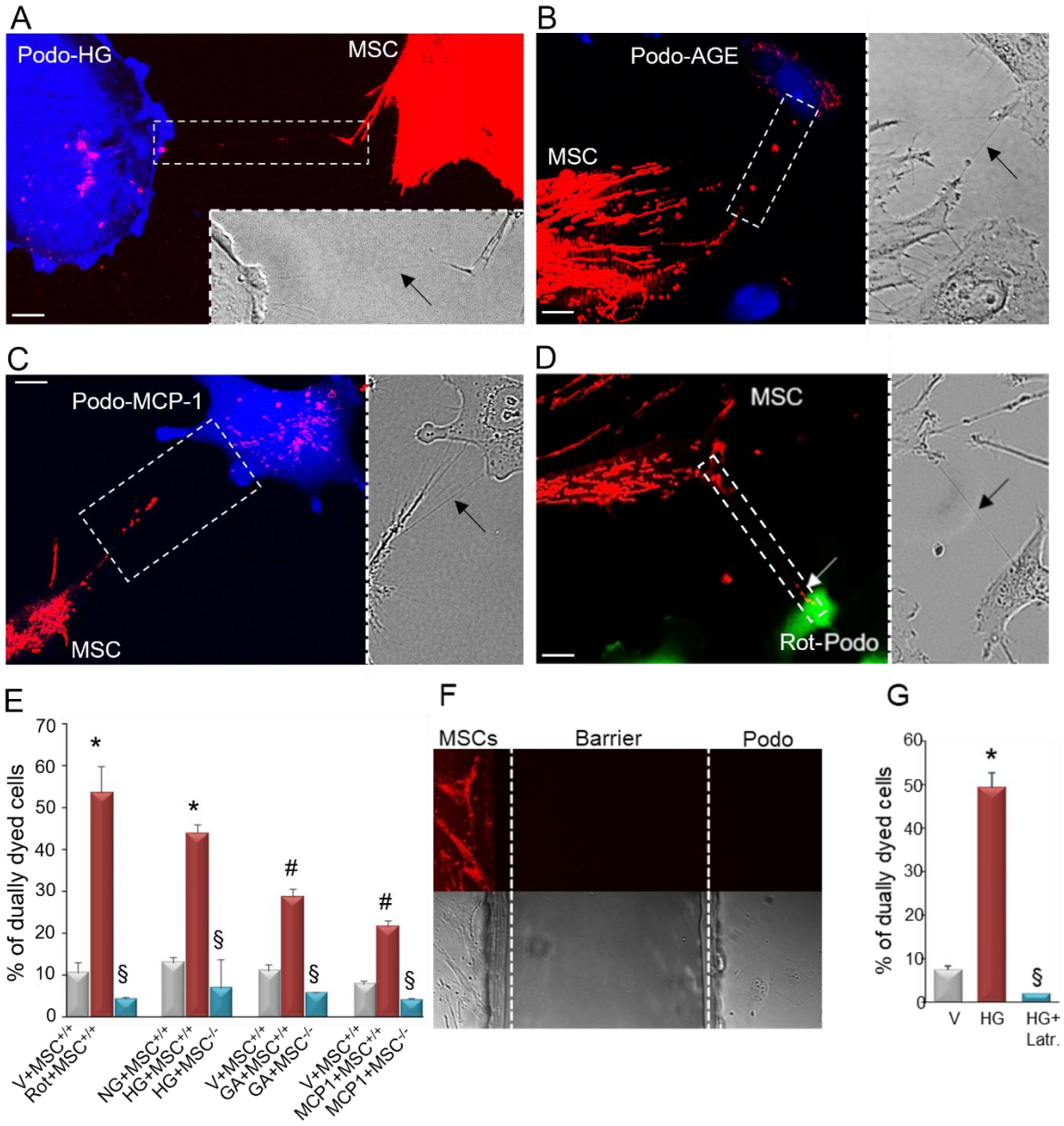

Figure 2. TNTs allow mitochondrial transfer from MSCs to podocytes pre-exposed to diabetes-related insults. Podocytes were pre-exposed to HG (25mM, 48h) **(A)**, GA (100 µg/ml, 72h) **(B)**, MCP-1 (10 ng/ml, 24h) **(C)**, or rotenone (100 nM, 24h) **(D)**. CellTracker Blue/Green-labelled podocytes were co-cultured with Cell-Light Mito-RFP-labelled MSCs. The images show RFP-mitochondria along TNTs and in the cytosol of podocytes (magnification X630, bar=50 µm, insert: DIC-image). **(E)** Podocytes were pre-exposed to rotenone (100 nM, 24h), HG (25 mM, 48h), GA (100 µg/ml, 72h), and MCP-1 (10 ng/ml, 24h) and then co-cultured with Cell-Light Mito-RFP-labelled MSCs. Experiments were performed using MSCs transfected with either M-Sec shRNA ($^{-/-}$) or a mock plasmid ($^{+/+}$). The graph shows the number of dually labelled podocytes (RFP and Green/Blue), (n=3, *$p<0.001$ Rot+MSC$^{+/+}$/HG+MSC$^{+/+}$ vs. V+MSC$^{+/+}$/NG+MSC$^{+/+}$; #$p<0.01$ GA+MSC$^{+/+}$/MCP-1+MSC$^{+/+}$ vs. V+MSC$^{+/+}$; §$p<0.05$ M-Sec$^{-/-}$ vs. V/NG+MSC$^{+/+}$). **(F)** HG-treated podocytes and donor MSCs, containing RFP-labeled mitochondria, were separately seeded in a 2-well Ibidi Culture Insert. After insert removal, the two populations, separated by a cell-free gap, were co-cultured for 24 hours under gentle shaking. As shown in the representative image, RFP-labeled mitochondria were not observed in recipient cells. **(G)** Efficiency of mitochondrial transfer from MSCs to HG-treated podocytes in the presence or absence of latrunculin-B (100 nM, 1h) (n=3, *$p<0.001$ HG vs. others; §$p<0.05$ HG+Latr. vs. vehicle).

4.3 TNT-mediated mitochondria transfer modifies the podocyte phenotype

To establish if transferred mitochondria can modify the podocyte phenotype, podocytes exposed to GA were co-cultured with green-labelled MSCs transfected with either M-Sec shRNA($^{-/-}$) or a mock plasmid ($^{+/+}$). Xenogenic mixed populations of primary murine podocytes and human MSCs have been used to obtain quantitative data. Exposure to GA induced both apoptosis and nephrin downregulation in podocytes and this effect was diminished by co-culturing podocytes with MSCs$^{+/+}$, while co-cultures with MSCs$^{-/-}$ failed to rescue podocytes (Figure 3A-C). Similarly, mitochondrial both gene expression (*ND4L, COX-1*) and membrane potential (MMP) were reduced, while mitochondrial oxidative stress enhanced in GA-treated podocytes and these effects were abolished exclusively in podocytes co-cultured with MSCs$^{+/+}$ (Figure 4 A-D). However, when podocytes were co-cultured with rotenone-treated MSCs (MSC^{Rot}), which carried altered mitochondria, there was no improvement in apoptosis, nephrin downregulation, and mitochondrial dysfunction, indicating that transfer of functional mitochondria is required to ameliorate the podocyte phenotype (Figure 3,4).

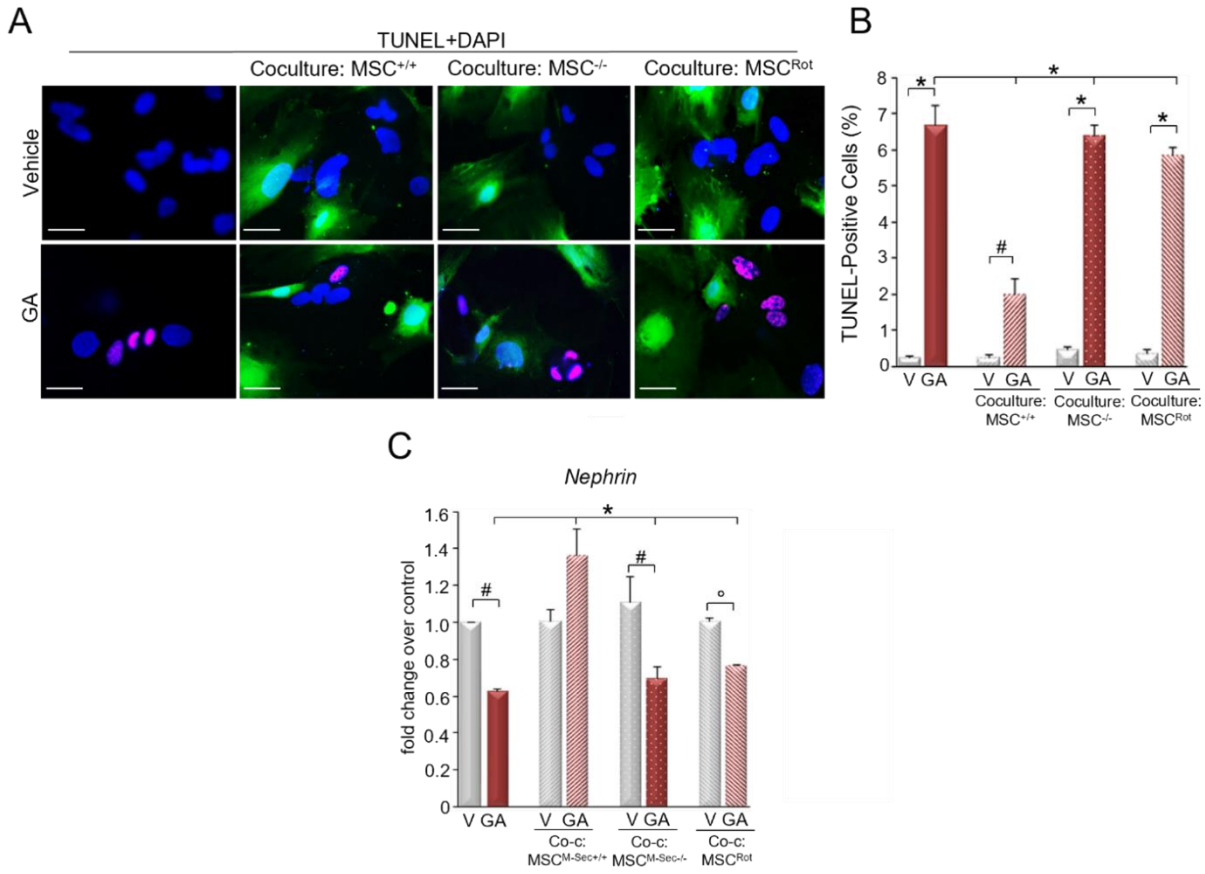

Figure 3. GA induced-podocyte apoptosis and nephrin downregulation is diminished by MSCs via M-Sec-TNT-mediated mitochondrial transfer. Murine podocytes were exposed to either vehicle or GA (100 µg/ml, 72h) and then co-incubated for 24 hours with MSCs. Experiments were performed using human MSCs transfected with either M-Sec shRNA ($^{-/-}$) or a mock plasmid ($^{+/+}$) or treated with rotenone (MSC^{Rot}). **(A)** Representative images of apoptotic podocytes (red) co-incubated with Cell Tracker-Green-labelled MSCs (magnification X400, bar=50 µm). Nuclei were stained with DAPI. **(B)** The graph shows the percentage of apoptotic podocytes (n=3, **p<0.001* GA vs. vehicle; GA-coculture-$MSC^{+/+}$ vs. GA, GA-coculture-$MSC^{-/-}$ and GA-coculture-MSC^{Rot}). Nephrin **(C)** mRNA levels were assessed by real time PCR in GA-treated podocytes. GAPDH served as housekeeping gene (n=3, *#p<0.01* GA vs. vehicle; *$p<0.01* GA-coculture-$MSC^{+/+}$ vs. GA, GA-coculture-$MSC^{-/-}$ and GA-coculture-MSC^{Rot}; **p<0.001* GA-coculture-$MSC^{+/+}$ vs. GA, GA-coculture-$MSC^{-/-}$ and GA-coculture-MSC^{Rot}).

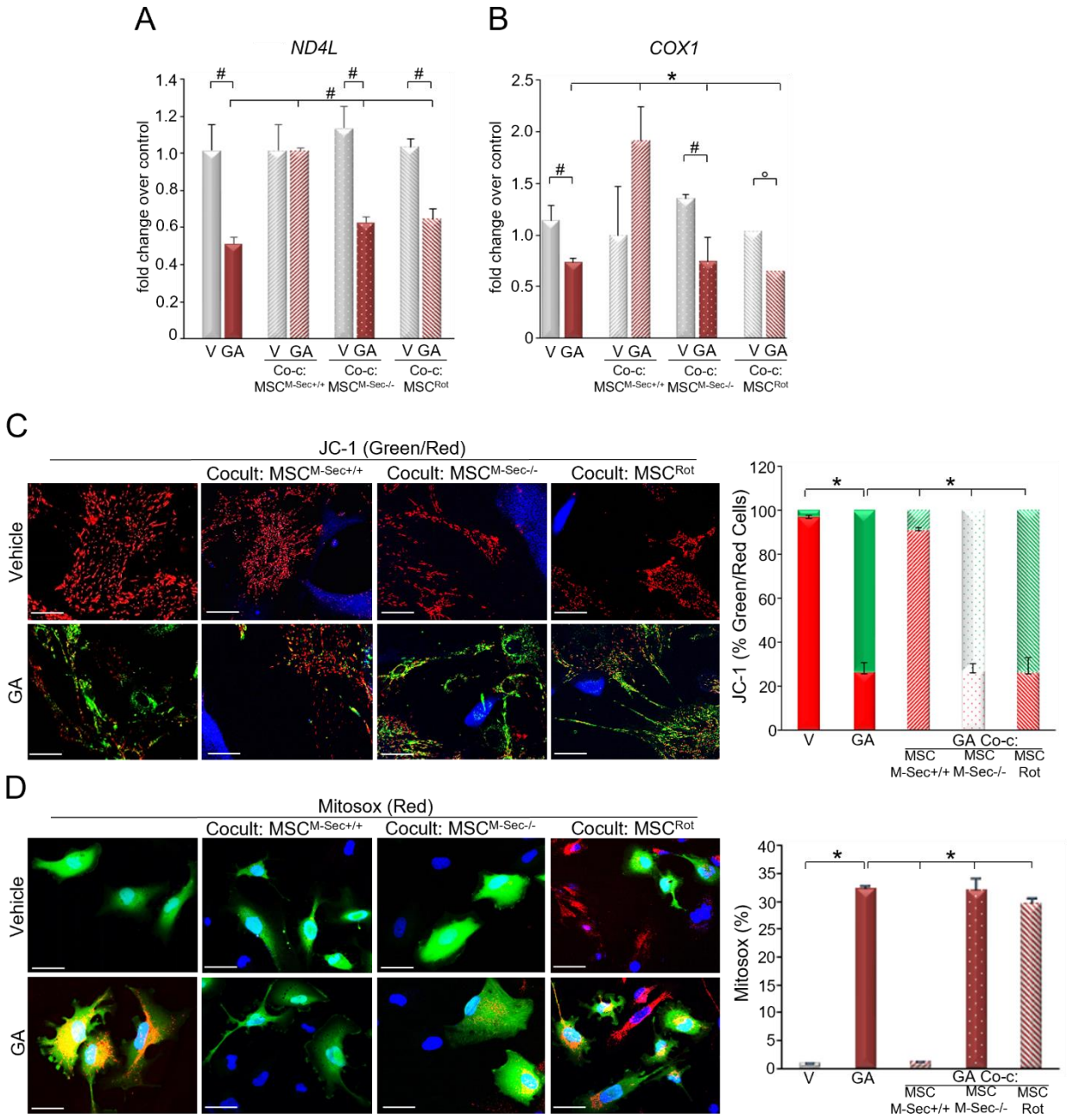

Figure 4. GA induced-mitochondrial dysfunction is diminished by MSCs via M-Sec-TNT-mediated mitochondrial transfer. Murine podocytes were exposed to either vehicle or GA (100 µg/ml, 72h) and then co-incubated for 24 hours with MSCs. Experiments were performed using human MSCs transfected with either M-Sec shRNA ($^{-/-}$) or a mock plasmid ($^{+/+}$), or treated with rotenone (MSC^{Rot}). ND4L **(A)**, and COX1 **(B)** mRNA levels were assessed by real time PCR in GA-treated podocytes. GAPDH served as housekeeping gene (n=3, *#p<0.01* GA vs. vehicle; *$p<0.01* GA-coculture-MSC$^{+/+}$ vs. GA, GA-coculture-MSC$^{-/-}$ and GA-coculture-MSC^{Rot}; **p<0.001* GA-coculture-MSC$^{+/+}$ vs. GA, GA-coculture-MSC$^{-/-}$ and GA-coculture-MSC^{Rot}). **(C)** Mitochondrial membrane potential was assessed using the fluorescence probe JC-1 in podocytes co-incubated with Cell Tracker-Blue-labelled MSCs (magnification X400, bar=50 µm). The graph shows quantification of red to green JC-1 fluorescence intensity (n=3; **p<0.001* GA vs. vehicle; GA-coculture-MSC$^{+/+}$ vs. GA, GA-coculture-MSC$^{-/-}$ and GA-coculture-MSC^{Rot}). **(D)** Mitochondrial oxidative stress was assessed using the fluorescent mitochondrial superoxide indicator MitoSoxRed in Cell Tracker-Green-labelled podocytes (magnification X200, bar=100 µm). The graph shows the percentage of fluorescent intensity per cell area (n=3, **p<0.001* GA vs. vehicle; GA-coculture-MSC$^{+/+}$ vs. GA, GA-coculture-MSC$^{-/-}$ and GA-coculture-MSC^{Rot}).

4.4 Diabetes affects the efficiency of MSCs as mitochondrial donors by reducing Miro1 expression

To clarify whether diabetes affects the efficiency of MSCs as mitochondrial donors, BM-MSCs were isolated by flushing the tibias and femurs of both diabetic (MSC^{DM}) and non-diabetic (MSC^{ND}) C57BL/6 mice after 14 weeks of diabetes (Figure 5 A,B). Cells were co-cultured with CellTracker-labelled podocytes that had been pre-exposed to HG. The next day, co-cultures were stained with WGA-Alexa Fluor 488 to reveal TNTs. Serial Z-stack images, acquired with a step-size of 0.25 μm, confirmed that TNTs did not adhere to the substrate. The number of TNTs interconnecting podocytes and MSC was significantly enhanced when podocytes were pre-exposed to HG, but was similar in HG-treated podocytes co-cultured with either MSC^{DM} or MSC^{ND} (Figure 5C), indicating that diabetes does not affect the ability of MSC to form TNTs with podocytes.

Experiments were then repeated co-culturing donors MSCs with RFP-labelled mitochondria with blue-labelled podocytes pre-exposed to HG. After 24 hours of co-cultures, cells were analysed by fluorescent microscopy. Quantification showed that TNT-mediated mitochondrial transfer was significantly diminished when podocytes were co-cultured with MSC^{DM}, despite the number of interconnecting TNTs was similar (Figure 5D), suggesting that diabetes can lower the efficiency of TNT-mediated mitochondrial transfer from MSCs.

To investigate whether diabetes affects Miro1 expression, we measured Miro1 mRNA levels by real-time PCR in both MSC^{DM} and MSC^{ND}. Miro1 expression was significantly reduced in MSC^{DM} compared to MSC^{ND}. Moreover, exposure of MSCs to diabetes-related insults, such as GA and MCP-1, significantly reduced Miro1 expression (Figure 6).

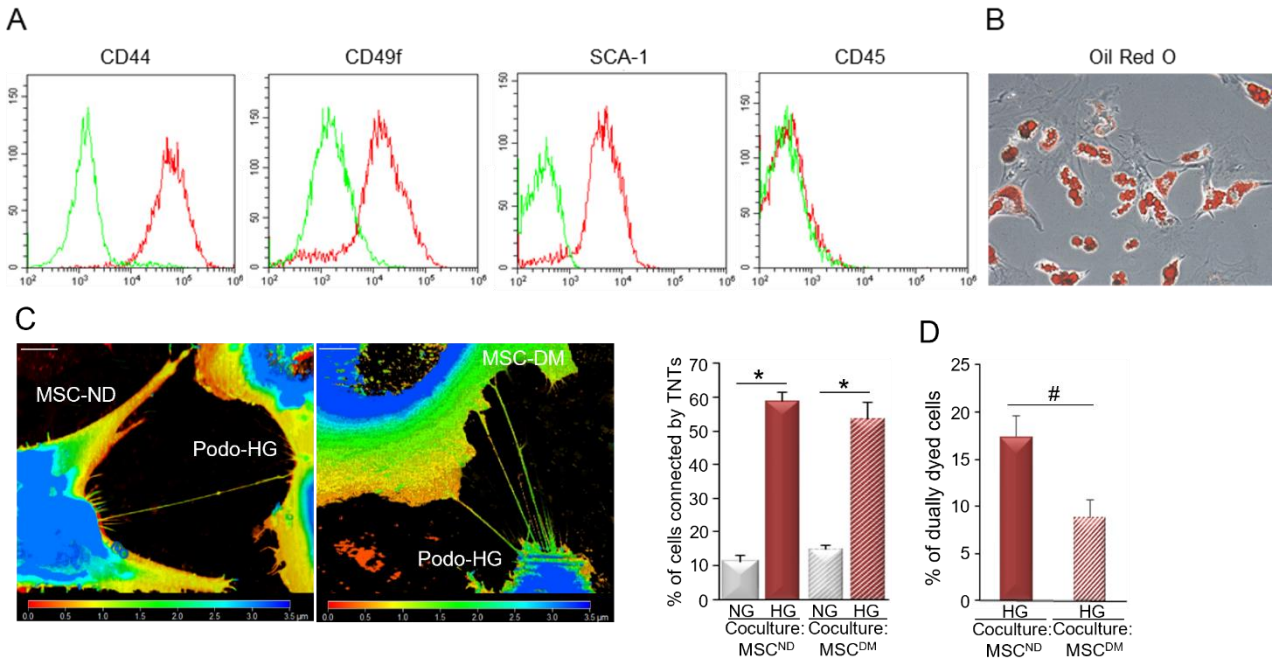

Figure 5. Diabetes diminished the efficiency of MSCs as mitochondrial donors. (A) BM-MSCs were CD44-, CD49f-, SCA-1-positive and CD45-negative as assessed by flow cytometry. **(B)** MSCs were cultured in Mesencult Adipogenic differentiation medium for 7 days. Oil Red O staining shows the presence of fat droplets in the cytosol indicating MSC differentiation into adipocytes. **(C)** Podocytes exposed to either NG or HG (25 mM, 48h) were stained with the CellTracker Blue and co-cultured with MSCs obtained from both non diabetic (MSC^{ND}) and diabetic (MSC^{DM}) mice. After 24 hours, co-cultures were stained with WGA-Alexa Fluor 488 to reveal TNTs. Serial Z-stack images acquired with a step-size of 0.25 µm proved that TNTs did not adhere to the substrate. A representative image showing a TNT, interconnecting a podocyte and a MSC (magnification X630, bar=50µm). Colours represent the Z-depth (depth-coding; red: bottom, blue: top). The percentage of podocytes and MSCs connected by TNTs is reported in the graphs (n=3, *$p<0.001$ HG-coculture-MSC^{ND} vs. NG-coculture-MSC^{ND}; HG-coculture-MSC^{DM} vs. NG-coculture-MSC^{DM}). **(D)** CellTracker Blue labelled podocytes, pre-exposed to HG (25mM, 48h), were co-cultured with Cell-Light Mito-RFP-labelled either MSC^{ND} or MSC^{DM} for 24 hours. The graph shows the number of dually labelled podocytes (RFP and Blue), (n=3, *$p<0.001$ HG-coculture-MSC^{ND} vs. HG-coculture-MSC^{DM}).

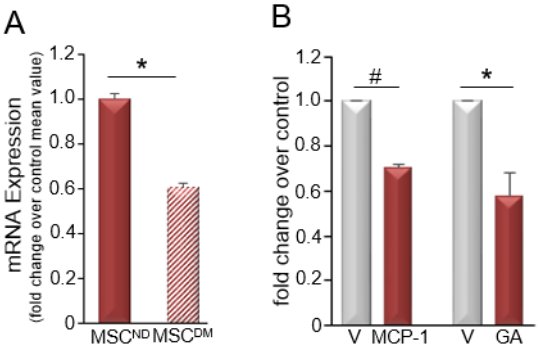

Figure 6. Diabetes diminished Miro1 expression in MSCs. Miro1 mRNA levels were assessed by real time PCR in MSC^{ND}/MSC^{DM} **(A)** and in MSCs treated with GA (100 µg/ml, 72h), MCP-1 (10 ng/ml, 24h) or vehicle **(B).** GAPDH served as housekeeping gene (n=3, *$p<0.001$ MSC^{DM} vs. MSC^{ND}; GA vs. vehicle; #$p<0.01$ MCP-1 vs. vehicle).

4.5 Miro1 overexpression re-establishes mitochondrial transfer efficiency and ameliorates mitochondrial parameters

To study the role of Miro1 in mitochondrial transfer, blue HG-treated podocytes were co-cultured with MSC^{DM} with labelled mitochondria and transfected either with an adenovirus expressing Miro1 ($MSC^{DM\text{-}Miro1}$) or mock vector ($MSC^{DM\text{-}Mock}$). Results showed that Miro1 overexpression in MSC^{DM} re-established mitochondrial transfer efficiency (Figure 7A).

To investigate the potential role of Miro1 overexpression on mitochondrial function, blue-labelled podocytes were treated with GA and then co-cultured with either $MSC^{DM\text{-}Mock}$ or $MSC^{DM\text{-}Miro1}$. Expression of the mitochondrial genes COX-1 and ND4L was assessed by real-time PCR in podocytes. Xenogenic mixed populations of human podocytes and murine MSCs have been used to obtain quantitative data. We found that Miro1 overexpression ameliorated GA-induced mitochondrial gene downregulation (Figure 7B,C). Moreover, there was a reduction in mitochondrial both oxidative stress and membrane potential in podocytes co-cultured with $MSC^{DM\text{-}Miro1}$ compared to control cells and control co-cultures (Figure 7D,E). Finally, GA-induced podocyte both apoptosis and nephrin downregulation were reduced in podocytes co-cultured with $MSC^{DM\text{-}Miro1}$ (Figure 7F,G).

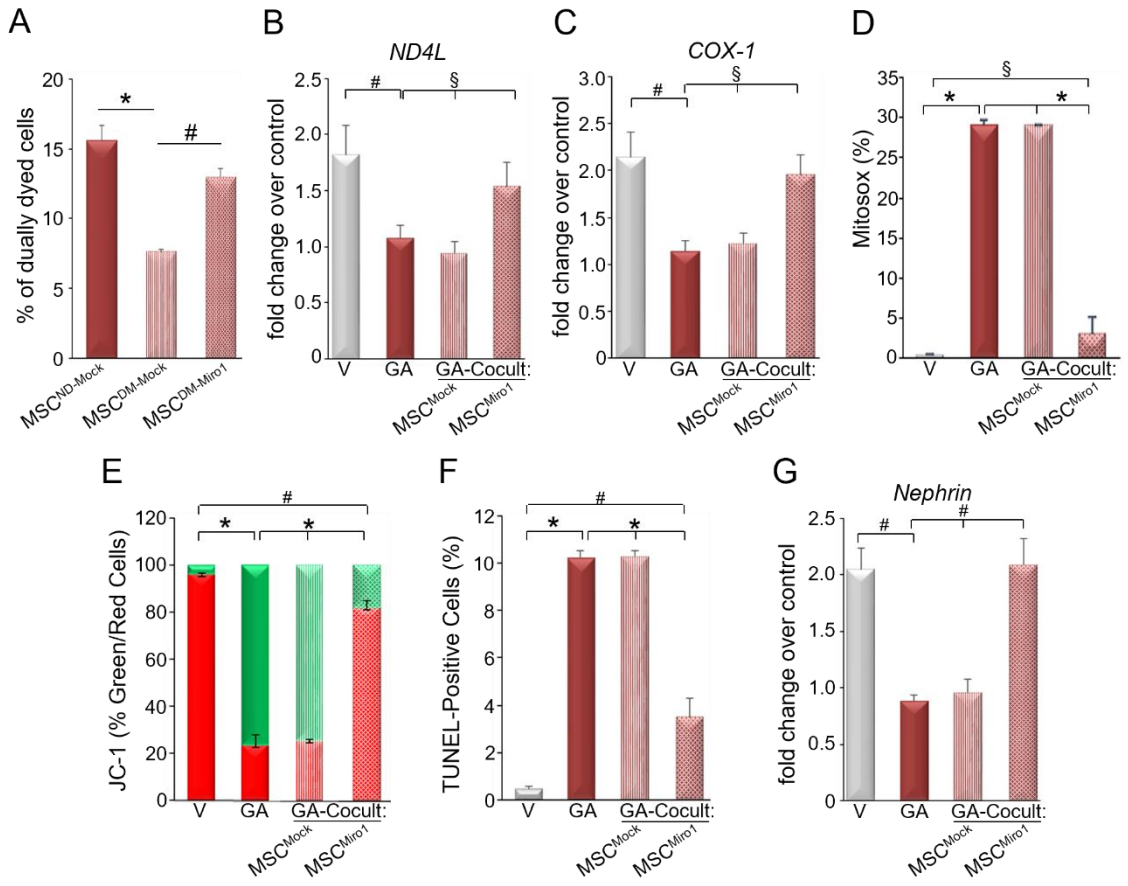

Figure 7. Diabetic MSCs overexpressing Miro1 rescued GA-treated podocytes. (A) HG-treated podocytes were co-cultured with MSC^{DM} transfected either with an adenovirus expressing Miro1 ($MSC^{DM\text{-}Miro1}$) or with a mock vector ($MSC^{DM\text{-}Mock}$). The graph shows the number of dually labelled podocytes (RFP and Blue) (n=3, *$p<0.001$ $MSC^{ND\text{-}Mock}$ vs. $MSC^{DM\text{-}Mock}$; #$p<0.01$ $MSC^{DM\text{-}Miro1}$ vs. $MSC^{DM\text{-}Mock}$. **(B,C)** GA-treated human podocytes (Cell Tracker-Blue) were co-cultured with MSC^{DM} either transfected with an adenovirus expressing Miro1 (^{Miro1}) or a mock vector (^{Mock}). COX-1 **(B)** and ND4L **(C)** mRNA levels were assessed by real time PCR in podocytes. GAPDH served as housekeeping gene (n=3, *$p<0.001$ GA vs. vehicle; §$p<0.05$ GA-coculture-MSC^{Miro1} vs. GA-coculture-MSC^{Mock} and GA). **(D)** Mitochondrial oxidative stress was assessed using the fluorescent mitochondrial superoxide indicator MitoSoxRed in podocytes. The graph shows the percentage of fluorescent intensity per cell area (n=3, *$p<0.001$ GA vs. vehicle and GA-coculture-MSC^{Miro1} vs. GA-coculture-MSC^{Mock} and GA; §$p<0.05$ GA-coculture-MSC^{Miro1} vs. vehicle). **(E)** The graph shows quantification of red to green JC-1 fluorescence intensity in podocytes. (n=3, *$p<0.001$ GA vs. vehicle and GA-coculture-MSC^{Miro1} vs. GA-coculture-MSC^{Mock} and GA; #$p<0.01$ GA-coculture-MSC^{Miro1} vs. vehicle). **(F)** The graph shows the percentage of apoptotic podocytes (n=3, *$p<0.001$ GA vs. vehicle and GA-coculture-MSC^{Miro1} vs. GA-coculture-MSC^{Mock} and GA; #$p<0.01$ GA-coculture-MSC^{Miro1} vs. vehicle). **(G)** Nephrin mRNA levels were assessed by real time PCR in human podocytes. GAPDH served as housekeeping gene (n=3, *$p<0.001$ GA vs. vehicle and GA-coculture-MSC^{Miro1} vs. GA-coculture-MSC^{Mock} and GA; #$p<0.01$ GA-coculture-MSC^{Miro1} vs. vehicle).

In vivo study

4.6 TNT-mediated mitochondria transfer from MSCs to glomerular cells in diabetic mice

To test if TNT-mediated transfer of mitochondria from exogenous MSCs to podocytes occurs *in vivo*, 8-week-old male C57BL/6 mice were made diabetic (DM) with streptozotocin (STZ). After eight weeks of diabetes, both DM and ND animals were injected (once a week for 6 weeks) with vehicle/mitochondria-GFP-tagged MSCs (1.0×10^4 cells/g body weight), which were obtained from either WT (MSC^{WT}) or M-Sec KO (MSC^{KO}) mice. After 14 weeks of diabetes, GFP-labelled-mitochondria were found in the glomeruli of $DM^{MSC\text{-}WT}$ mice, while they were not observed in ND animals and were rarely seen in $DM^{MSC\text{-}KO}$ mice. Double immunofluorescence with nephrin confirmed the presence of GFP-labelled mitochondria within podocytes, proving that mitochondrial transfer from MSCs to podocytes occurs *in vivo* via a M-Sec-dependent mechanism (Figure 8).

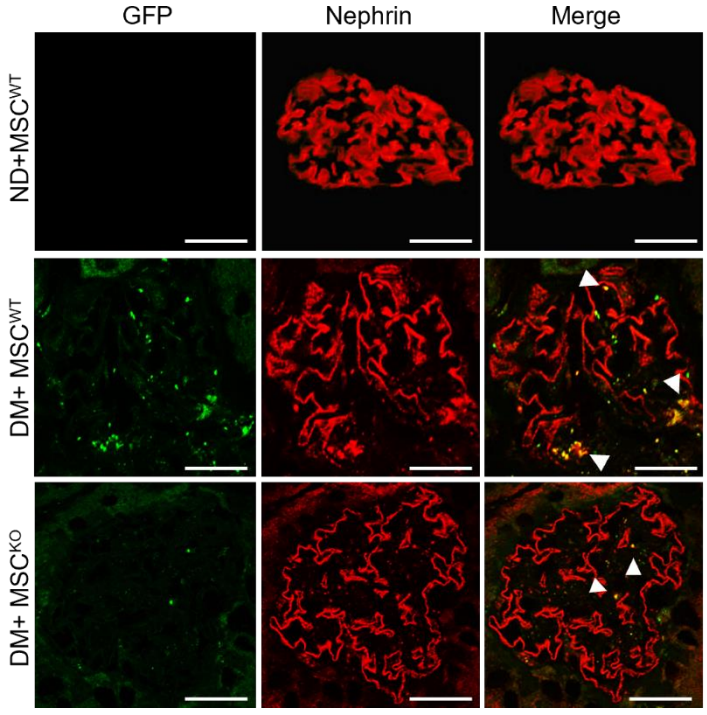

Figure 8. Exogenous MSCs transfer mitochondria to podocytes *in vivo* in experimental diabetes via a M-Sec-dependent mechanism. After eight weeks of diabetes, diabetic (DM) and non-diabetic (ND) mice were treated for 6 weeks with CellLight Mitochondria-GFP-labelled MSCs from WT (MSC^{WT}) and M-Sec KO mice (MSC^{KO}) (1.0×10^4 cells/g body weight, weekly) for 6 consecutive weeks. Double immunofluorescence for GFP and the podocyte marker nephrin was performed on renal cortex sections. Merged images showed colocalization (original magnification X400, bars=50 µm).

4.7 Effect of MSC-mediated mitochondria transfer on metabolic and physiological parameters, albuminuria and renal function

After 8 weeks of STZ-induced diabetes, levels of albuminuria were significantly greater in DM compared to ND mice, indicating the development of early DN [ND: 17.24 (15.4-18.7) vs. DM: 35.73 (28.40-45.51); $p<0.01$]. Animals with comparable levels of albuminuria were allocated to the different treatment groups (DM/ND$^{MSC\text{-}WT}$, DM/ND$^{MSC\text{-}KO}$, vehicle) as described above.

Table 1 shows both metabolic and physiological parameters assessed at the end of MSC treatment in all groups. Blood glucose and glycated haemoglobin were significantly higher and body weight significantly lower in DM mice. Treatment with either MSC^{WT} or MSC^{KO} did not alter these parameters. DM mice showed a six-fold increase in ACR compared to ND animals. The rise in ACR was reduced by 62% in DM$^{MSC\text{-}WT}$, but not in DM$^{MSC\text{-}KO}$. Moreover, diabetes-induced renal function decline was ameliorated exclusively in DM$^{MSC\text{-}WT}$.

Table 1. General assessment parameters in each of the studied groups.

	Body weight (g)	BG (mg/dl)	Glycated Hb (%)	sBP (mmHg)	ACR (µg/mg)	CrCl (µg/mg)
ND	30.0 ± 1.4	135.4 ± 4.2	4.4 ± 0.3	118.5 ± 7.0	29.2 ± 4.7	0.57 ± 0.14
ND+ MSC-WT	30.3 ± 1.1	166.2 ± 0.6	5.5 ± 0.5	105.4 ± 7.6	31.4 ± 5.4	0.62 ± 0.10
DM	22.7 ± 0.98[a]	491.4 ± 49.4[a]	11.5 ± 0.3[a]	112.6 ± 3.5	179.1 ± 12.0[a]	0.19 ± 0.02[d]
DM+ MSC-KO	24.5 ± 0.9[a]	488.2 ± 42.8[a]	11.1 ± 0.6[a]	110.2 ± 6.8	162.5 ± 14.1	0.15 ± 0.03[d]
DM+ MSC-WT	24.0 ± 0.5[a]	518.4 ± 42.4[a]	11.8 ± 0.3[a]	102.4 ± 9.6	67.6 ± 10.5[b,c]	0.40 ± 0.09[e]

Data are shown as mean ± SEM. ND: non-diabetic; DM: diabetic; BG: blood glucose; sBP: systolic blood pressure. [a]$p<0.001$ DM groups vs. ND groups; [b]<0.001 DM+MSC^{WT} vs. DM and DM+MSC^{KO}; [c]$p<0.05$ DM+MSC^{WT} vs. ND groups. [d]$p<0.01$ DM and DM+MSC^{KO} vs. ND groups; [e]$p<0.05$ DM+MSC^{WT} vs. DM and DM+MSC^{KO}.

4.8 Podocyte and structural abnormalities

To evaluate the effect of MSCs on podocyte injury, both nephrin and podocin mRNA and protein expression were assessed by immunofluorescence and real-time PCR on renal cortex and cortical renal sections, respectively. Diabetes-induced both nephrin and podocin downregulation were reduced by treatment with MSC^{WT}, while MSC^{KO} injection was ineffective (Figure 9 A-E).

PAS staining was performed to determine the effect of MSCs on the extent of the glomerular damage. As shown in Figure 10, the mild mesangial expansion observed in DM animals, was reduced exclusively by treatment with MSC^{WT} (Figure 10 A,B). Consistently, diabetes-induced both fibronectin and collagen overexpression was ameliorated in DM mice receiving MSC^{WT}, but not MSC^{KO} cells (Figure 10 C-F).

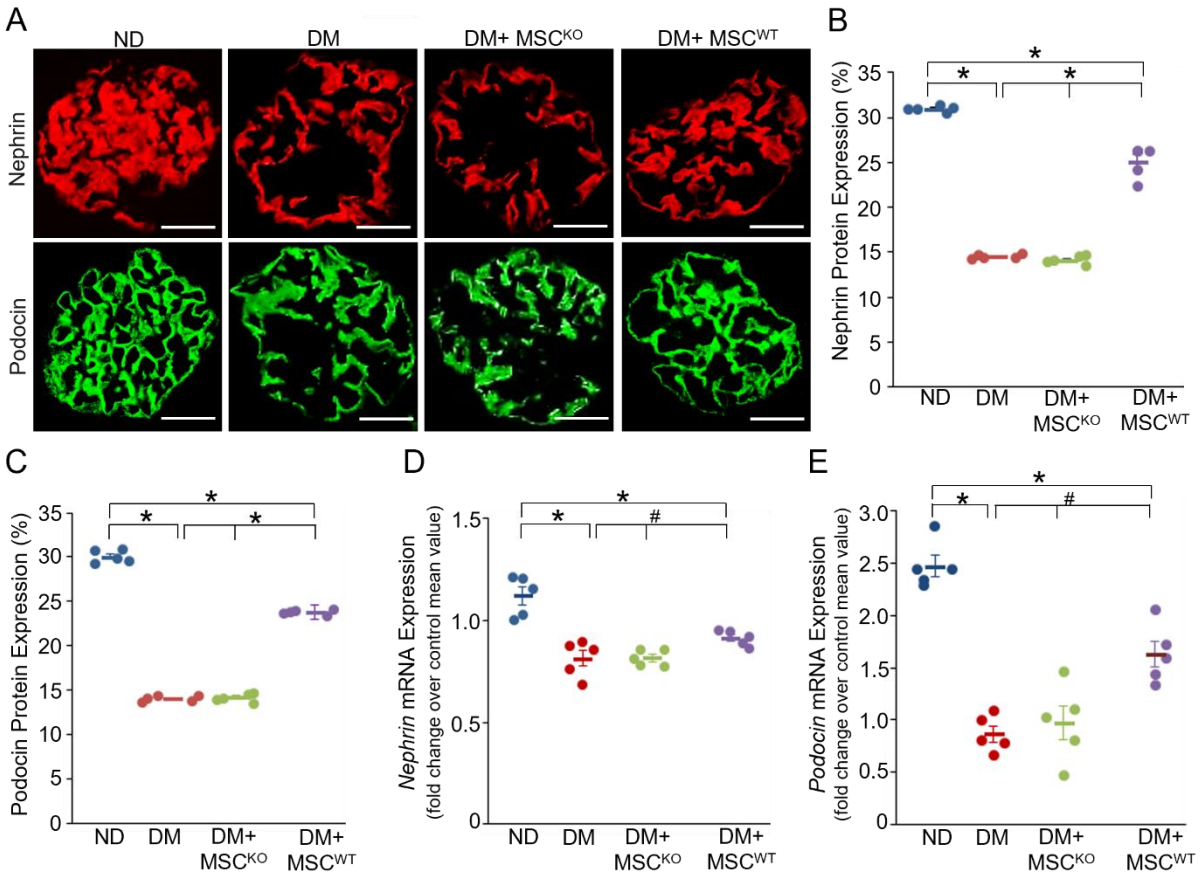

Figure 9. Effect of treatment with exogenous MSCs on diabetes-induced both nephrin and podocin downregulation. After eight weeks of diabetes, non-diabetic (ND) and diabetic (DM) mice were treated with MSC^{WT}, MSC^{KO}, or vehicle for 6 weeks. Both nephrin and podocin mRNA and protein expression were assessed by immunofluorescence and real time PCR. **(A)** Representative immunofluorescence images of nephrin and podocin are shown (magnification X400, bars=50µm). **(B, C)** Quantification of both nephrin and podocin glomerular staining is reported in the graphs (*$p<0.001$ DM vs. ND and DM+MSC^{WT} vs. others). **(D, E)** Nephrin and podocin mRNA levels were measured by real-time PCR on total RNA extracted from the renal cortex. Results were corrected for the expression of WT-1 (*$p<0.001$ DM vs. ND and DM+MSC^{WT} vs. ND; #$p<0.05$ DM+MSC^{WT} vs. DM and DM+MSC^{KO}).

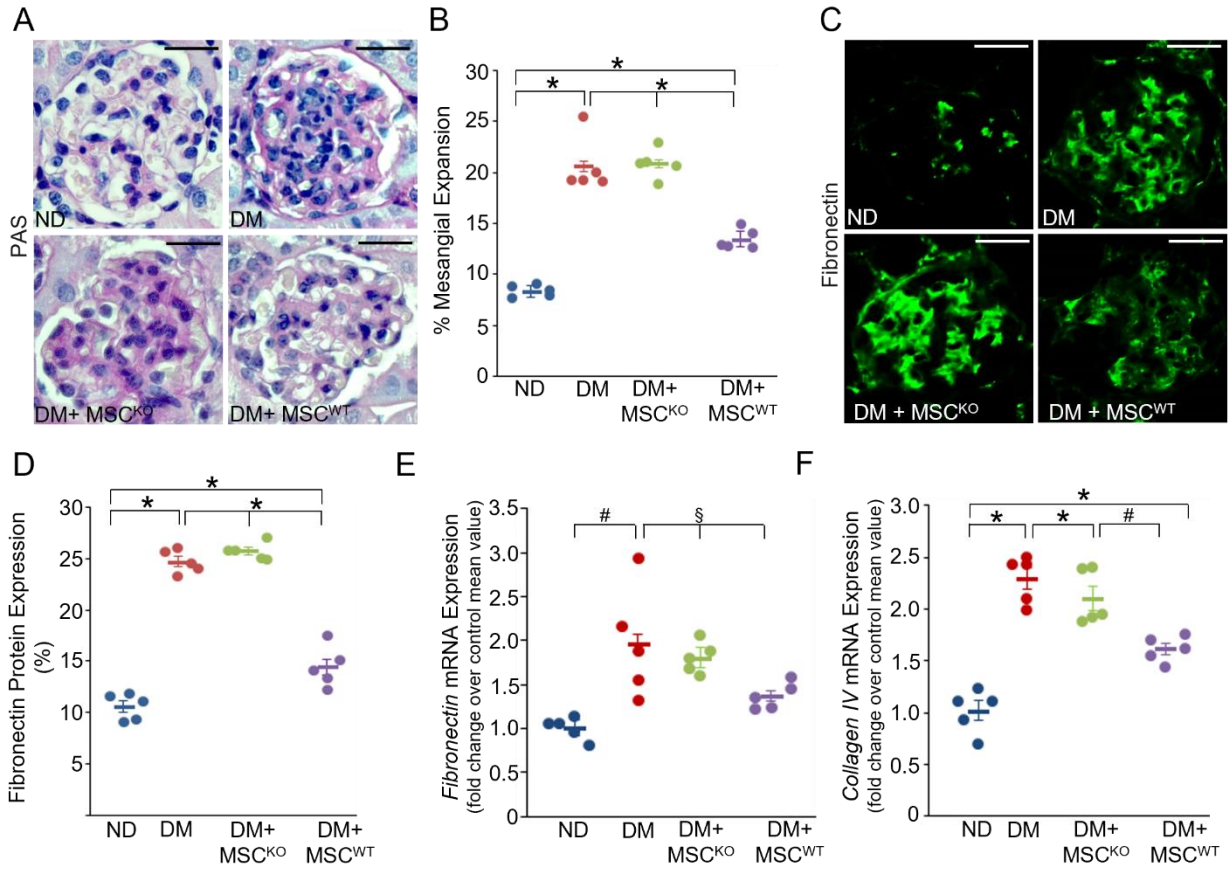

Figure 10. Effect of treatment with exogenous MSCs on diabetes-induced both mesangial expansion and extracellular matrix component expression. (A, B) PAS staining was assessed in renal cortex sections. Representative images (magnification X400, bars=50µm) and percentage PAS glomerular-positive areas are shown (*$p<0.001$ DM vs ND and DM+MSC^{WT} vs. others). **(C)** Representative immunofluorescence images of fibronectin are shown (magnification X400, bars=50µm). **(D)** Quantification of fibronectin glomerular staining is reported in the graph (*$p<0.001$ DM vs. ND and DM+MSC^{WT} vs. others). **(E, F)** Fibronectin and collagen IV mRNA levels were measured by real-time PCR on total RNA extracted from the renal cortex. Results were corrected for the expression of the housekeeping gene HPRT [(fibronectin: #$p<0.01$ DM vs. ND; §$p<0.05$ DM+MSC^{WT} vs. DM and DM+MSC^{KO}) (ColIV *$p<0.001$ DM vs. ND and DM+MSC^{WT} vs. others).

4.9 Mitochondrial dysfunction

We next investigated the effect of MSCs on mitochondria function. Diabetes reduced the expression of the mitochondrial transcription factor/genes (TFAM, COX1, ND4L), while expression of genes controlling mitochondrial biogenesis, fusion, fission and mitophagy was unaltered. Treatment with MSC^{WT} ameliorated/abolished TFAM, COX1, and ND4L downregulation, whereas MSC^{KO} injection was ineffective (Figure 11).

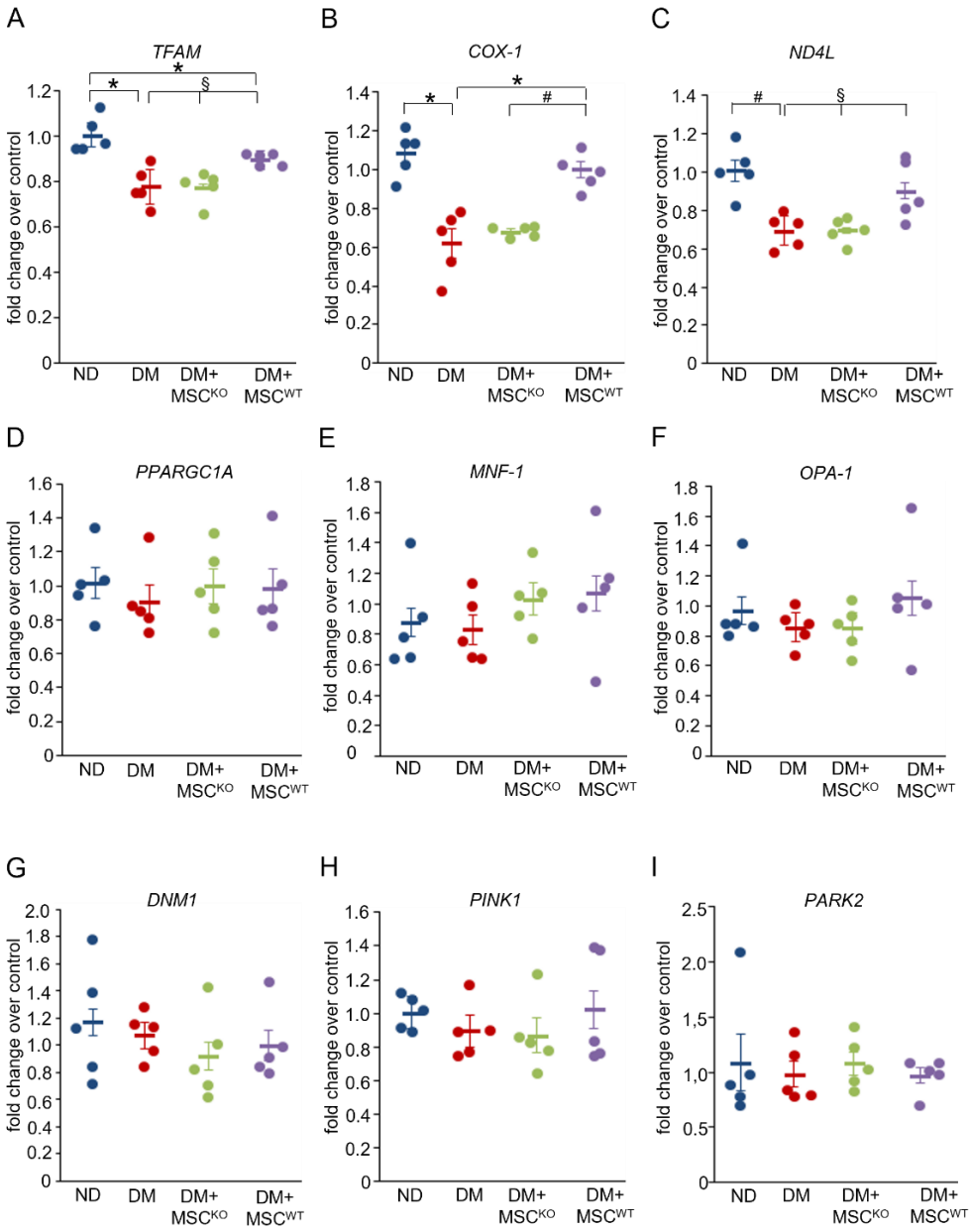

Figure 11. Effect of treatment with exogenous MSCs on diabetes-induced mitochondrial dysfunction. After eight weeks of diabetes**,** non-diabetic (ND) and diabetic (DM) mice were treated with either MSC^{WT}, MSC^{KO}, or vehicle for 6 weeks. TFAM **(A)**, COX.1 **(B)**, ND4L **(C)**, PPARGC1A **(D)**, MNF-1 **(E)**, OPA-1 **(F)**, DNM1 **(G)**, PINK1 **(H)**, and PARK2 **(I)** mRNA levels were measured by real-time PCR on total RNA extracted from the renal cortex. Results were corrected for the expression of the housekeeping gene HPRT. [(TFAM: **p<0.001*; ND vs. DM and DM+MSC^{WT}; *§p<0.05* DM+MSC^{WT} vs. DM and DM+MSC^{KO}) (COX-1: **p<0.001*; DM vs. ND and DM+MSC^{WT}; *#p<0.01* DM+MSC^{WT} vs. DM+MSC^{KO}) (ND4L: DM vs. ND; *§p<0,05* DM+MSC^{WT} vs. DM and DM+MSC^{KO}).

4.10 Markers of inflammation

We then assessed whether MSCs administration has beneficial effects on inflammation in experimental diabetes. The number of macrophages (MAC-2^+ cells) within the glomeruli was significantly greater in DM compared to ND mice and this effect was ameliorated by both MSC^{WT} and MSC^{KO} treatment (Figure 12 A,B). As the chemokine MCP-1 plays a key role in monocyte accrual, we assessed the expression of MCP-1 and its cognate receptor CCR2. We found that diabetes-induced MCP-1 and CCR2 mRNA overexpression was abolished by both MSC^{WT} and MSC^{KO} treatment, likely via a M-Sec-TNT-independent paracrine mechanism (Figure 12 C,D).

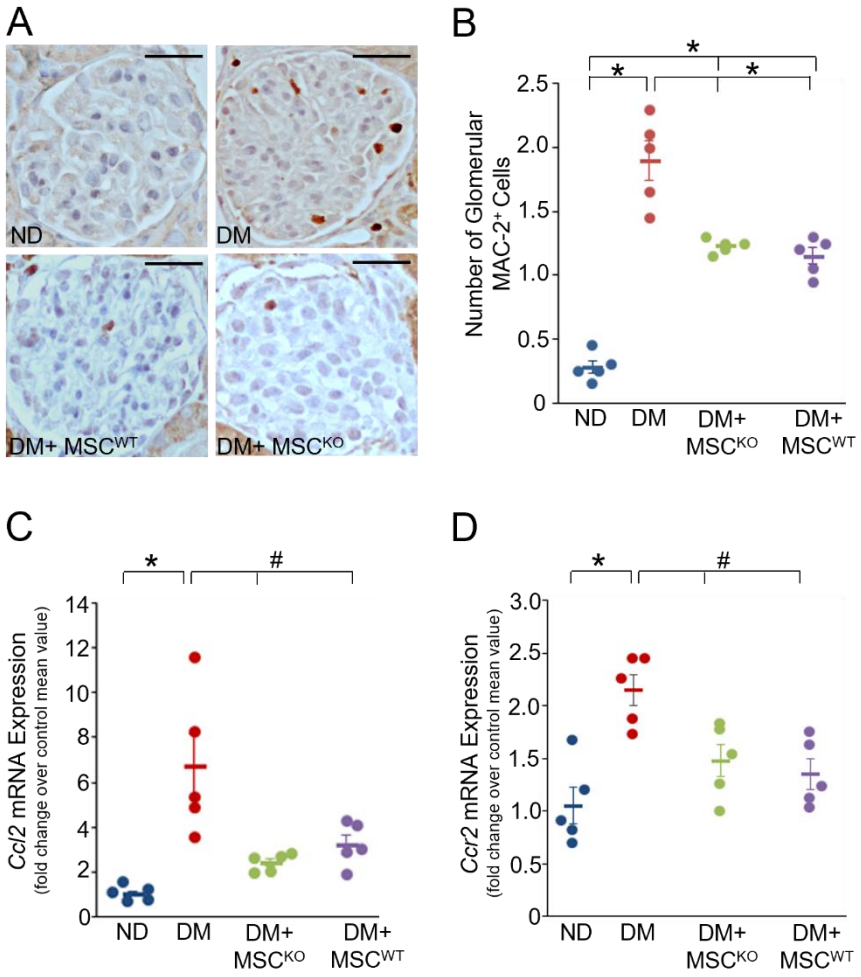

Figure 12. Effect of MSCs on markers of inflammation. After eight weeks of diabetes**,** non-diabetic (ND) and diabetic (DM) mice were treated with MSC^{WT}, MSC^{KO}, or vehicle for 6 weeks. **(A,B)** Representative images of glomerular MAC-2 positive immunostaining are shown and quantitation reported in the graph (magnification X400, bars=50µm) (*$p<0.001$* DM vs. ND and DM+MSC^{WT} vs. others). MCP-1/CCL2 **(C)** and CCR2 **(D)** mRNA levels were measured by real-time PCR on total RNA extracted from the renal cortex. Results were corrected for the expression of HPRT (*$p<0.001$* DM vs. ND; *#$p<0.01$* DM vs. DM+MSC^{KO} and DM+MSC^{WT}).

5. Discussion

In this study, we have provided evidence that MSCs can ameliorate diabetes-induced podocyte injury through TNT-M-Sec-mediated mitochondrial transfer; however, diabetes alters this cytoprotective mechanism by reducing the efficiency of endogenous MSCs as mitochondrial donors.

Several both *in vitro* and *in vivo* findings support this notion. TNT formation occurred between MSCs and podocytes in a M-Sec-dependent manner and it was enhanced by podocyte exposure to diabetes-related insults. TNTs were functionally active as exposure of podocytes to diabetes-related insults increased TNT-M-Sec-mediated unidirectional mitochondrial transfer from MSCs towards podocytes, resulting in podocytes repair. Diabetes affected the efficiency of MSCs as mitochondria donors by reducing Miro1 expression and overexpression of Miro1 in MSCs not only re-established their efficiency as mitochondria donors, but also ameliorated mitochondrial parameters in recipient podocytes. Transfer of mitochondria from exogenous MSCs to podocytes also occurred *in vivo* in diabetic mice. Moreover, in diabetic mice with established DN, treatment with exogenous MSCs ameliorates albuminuria, renal function, slit diaphragm protein down-regulation, mesangial expansion, and downregulation of mitochondria-related genes in a M-Sec-dependent manner.

The protective effect of exogenous MSCs in DN has been previously reported in various experimental models of diabetes[130,131,132] but the underlying mechanisms remain poorly defined. Exogenous MSCs are unlikely to replace damaged renal cells and paracrine mechanisms are believed to be important in renal protection. Herein, we provide evidence of an important role of TNTs in explaining the beneficial effects of MSCs. TNTs are membrane channels bridging distant cells and allowing intercellular exchange of various cargos. Previous studies showed that MSCs form TNTs with several cell types, including corneal epithelial cells[142], airway epithelial cells[138], brain epithelial cells[114], pulmonary alveoli[108], cardiomyocytes[143,144], macrophages[145], and endothelial cells[113]. Our results show that podocytes can also connect with MSCs via intracellular membrane bridges that fulfil the morphological criteria for the definition of TNTs. Specifically, these membranous structures were straight, exhibited a width of less than 0.5 μm and a length of several cell diameters, and contained a F-actin/tubulin backbone[79]. Moreover, these TNT-like structures did not adhere to the substrate and this is a specific feature of TNTs that differentiate them from filopodia[146]. Although TNTs have been shown predominantly *in vitro*, recent studies have demonstrated TNT-like structures *in vivo* in retinal pericytes, and in models of Dent disease and obstructive nephropathy[93,147,148,] confirming that TNTs are not only *in vitro* "artefacts".

TNTs form *de novo* predominantly from stressed cells and our results demonstrate that the cellular stress induced by exposure of podocytes to high glucose, MCP-1, and GA was sufficient to trigger TNT formation between podocytes and MSCs. High glucose-induced TNT formation was previously reported in both MC3T3 osteoblast[149] and mesothelial cells[150]. Importantly, diabetes-induced TNT formation between podocytes and MSCs was almost abolished by M-Sec silencing, indicating a M-Sec-dependent effect. Consistent with this, previous studies have shown that M-Sec cooperates with the RalA small GTPase and the exocyst complex to trigger F-actin polymerization and TNT formation[80,151]. In particular, Zhang Y *et al.* reported that M-Sec is involved in TNT formation between MSCs and cardiomyocytes[152] and we recently showed the key role of M-Sec in TNT formation between podocytes[123]. On the contrary, tubular renal cells form TNTs in a M-Sec-independent manner.

Stress-induced TNT formation may be considered as a defence mechanism whereby injured cells can replace dysfunctional organelles. In our study, we demonstrated that MSCs could transfer mitochondria to injured podocytes. Silencing of M-Sec as well as treatment with the F-actin depolymerizing drug latrunculin-B, prevented mitochondrial transfer from MSCs to podocytes, confirming that the exchange occurred via TNTs. Consistent with our findings, MSCs were shown to transfer mitochondria through a TNT-mediated mechanism with various other cell types, such as cardiomyocytes[118], endothelial cells[140], pulmonary alveolar epithelial cells[138], renal tubular cells[111], and macrophages[145]. Although mitochondria are large organelles, mitochondrial transfer through TNTs is feasible as mitochondria can enlarge TNTs, creating a bulge.

Mitochondrial transfer from MSCs to podocytes was enhanced when podocytes were exposed to either rotenone or diabetes-related insults. This suggests that transfer was aimed to rescue podocytes with dysfunctional mitochondria. In keeping with this, mitochondrial transfer from MSCs to podocytes abolished GA-induced downregulation of mitochondrial genes as well as the rise in both MMP and mitochondrial oxidative stress in response to GA. Importantly, mitochondrial transfer also abrogated GA-induced both apoptosis and nephrin downregulation, confirming the key role of mitochondrial dysfunction in the podocyte injury. On the contrary, MSCs lacking M-Sec and thus, unable to form TNTs, failed to show any benefit, supporting the notion that a TNT-mediated mechanism underlies the protective effect of MSCs.

Beside mitochondria, TNTs also allow exchange of other organelles, cellular components, and signalling molecules between connected cells. However, donor MSCs with dysfunctional mitochondria failed to protect injured podocytes, indicating that rescuing of damaged podocytes required transfer of healthy mitochondria. Today, TNTs are considered the predominant mechanism of both horizontal mitochondrial exchange and “intercellular” mitochondrial quality control[153].

Mechanisms allowing mitochondrial replacement are of particularly relevance in cells, as podocytes, that are terminally differentiated. Indeed, mitochondrial damage tends to accumulate in cells that cannot replicate.

Studies performed in cardiomyocytes have shown that the efficiency of MSCs as mitochondrial donors strongly depends on Miro1 expression. Miro1 is a mitochondrial Rho-GTPase that is responsible for mitochondrial association with the microtubule mobility complex and drives the movement of mitochondria along TNTs[139]. Accordingly, iPSC-MC cells that have greater Miro1 expression outperform MSC as mitochondrial donor to cardiomyocytes[152]. In our study, we found a reduction of both Miro1 expression and mitochondrial transfer in MSCs isolated from diabetic animals. This suggests that diabetes can hamper this important mechanism of TNT-mediated mitochondrial replacement. The observation that exposure of MSCs to both GA and MCP-1 downregulates Miro1 provides a potential mechanism by which diabetes may affect Miro1 expression *in vivo*.

Notably, Miro1 overexpression not only re-established the efficiency of MSCs as mitochondrial donors, but also led to a significant improvement in GA-induced podocyte injury. Consistent with our findings, previous studies showed that bioengineered MSCs that overexpress Miro1 had greater mitochondrial donor capacity and were therapeutically more effective in experimental models of airway injury, asthma[138], stroke[115] and anthracycline-induced cardiomyopathy[152].

Our *in vivo* study in STZ-induced diabetes demonstrates that exogenous MSCs can transfer mitochondria to podocytes via a M-Sec-dependent mechanism. MSCs carrying GFP-mitochondria were administered intravenously at the dose of 1.0×10^4 cells/g body weight on the basis of previous studies showing efficacy of this dose in experimental diabetes[134,154]. In diabetic mice with established albuminuria, GFP-mitochondria from MSC^{WT} were found predominantly in podocytes as demonstrated by colocalization with nephrin. This phenomenon was not observed in ND animals, indicating that transfer only occurs towards injured cells. Notably, mitochondria were rarely seen in the glomeruli of diabetic mice treated with MSC^{KO}, proving that M-Sec is required for mitochondrial transfer. A previous study by Konari N. *et al*. has shown mitochondria transfer from MSCs to proximal tubular epithelial cells in experimental DN[154], but the underlying mechanism was not elucidated.

After 14 weeks of diabetes, there was a 6-fold increase in albuminuria in diabetic mice compared with controls. Treatment with MSC^{WT} reduced albuminuria by 50%. Administration of MSCs did not affect blood glucose levels, glycated haemoglobin, and blood pressure in diabetic mice; therefore, the beneficial effect on albuminuria of MSCs was not due to amelioration of metabolic/hemodynamic

control. Consistent with our results, Wang *et al*. reported a metabolic-independent protective effect of MSCs in diabetic animals[130]. By contrast, other studies showed amelioration of blood glucose control in MSCs-treated diabetic animals[130,131]. Discrepancies may be due to differences in experimental models, diabetes duration, and MSCs both dose and administration route.

Treatment with MSC^{WT} significantly reduced diabetes-induced both nephrin and podocin downregulation. Slit diaphragm (SD) and SD-associated proteins play a key role in the pathogenesis of proteinuria[155] and nephrin downregulation is a characteristic feature of human DN[156]. Therefore, prevention of SD protein loss is a likely mechanism of the anti-proteinuric effect of MSCs.

Structural analysis showed amelioration of mesangial expansion in diabetic mice treated with MSC^{WT}. This was paralleled by a reduction in both fibronectin and collagen IV deposition. Podocyte damage/loss can lead to glomerulosclerosis[157]. Therefore, rescue of podocytes may provide explanation for the anti-fibrotic effects of MSCs.

Mitochondrial dysfunction plays an important role in the development of DN[57] and expression of TFAM, COX1, and ND4L was reduced in diabetic mice compared to controls. This effect was reduced by administration of MSC^{WT} in agreement with previous studies in other animal models[158,159]. Moreover, these results support the hypothesis that amelioration of experimental DN by MSC may be at least in part ascribed to mitochondria replacement.

Importantly, the beneficial effect of exogenous MSCs on albuminuria, renal function, SD protein loss, mesangial expansion, and expression of mitochondria-related genes was not observed in mice treated with MSC^{KO}. This suggests that the TNT-M-Sec system is important in explaining the efficacy of MSC-based therapy in experimental DN. However, we cannot exclude the possibility that TNT-independent mechanisms may also contribute to the protective effect of exogenous MSCs expressing M-Sec. M-Sec interacts with small GTPases[80] regulating the actin cytoskeleton; therefore, M-Sec deficiency may alter MSC actin dynamics. In addition, loss of M-Sec, which is a retinoic acid target[160], may interfere with MSC differentiation. However, donor MSCs carrying altered mitochondria were unable to rescue the apoptosis of recipient podocytes suggesting that MSCs expressing M-Sec protect podocytes predominantly via TNT-mediated mitochondrial transfer.

Amelioration of diabetes-induced both glomerular monocyte infiltration and overexpression of markers of inflammation was observed not only in mice treated with MSC^{WT}, but also in animals treated with MSC^{KO}. Therefore, the anti-inflammatory effect of MSCs was M-Sec-independent and likely due to either a paracrine mechanism or exosomes. Reduction of both inflammatory cytokines and macrophage infiltration in response to intravenous injection of MSCs has been previously

reported in experimental DN[131]. Moreover, Nagaishi *et al.* reported that MSC therapy ameliorated experimental DN via the paracrine effect of renal trophic factors including exosomes[134].

In conclusion, this study provided the first evidence that TNT-mediated exchange of mitochondria from BM-MSCs to podocytes occurs both *in vitro* and *in vivo* in the context of diabetes. This transfer rescues diabetes-injured podocytes and ameliorates experimental DN. However, diabetes alters this cytoprotective mechanism by downregulating Miro1 in endogenous MSCs. Enhancing the efficiency of diabetic MSCs as mitochondrial donors by modulating Miro1 expression may represent a new therapeutic strategy in DN and possibly in other chronic complications of diabetes.

References

1. Levin, A. *et al.* Global kidney health 2017 and beyond: a roadmap for closing gaps in care, research, and policy. *The Lancet* vol. 390 1888–1917 (2017).
2. Alicic, R. Z. *et al.* Diabetic kidney disease: Challenges, progress, and possibilities. *Clin. J. Am. Soc. Nephrol.* **12**, 2032–2045 (2017).
3. Ritz, E. *et al*. Clinical manifestation and Natural History of Diabetic Nephropathy. *Clin. Featur. Diabet. Nephrop.* **170**, 19–27 (2011).
4. Afkarian, M. *et al.* Clinical Manifestations of Kidney Disease Among US Adults With Diabetes, 1988–2014. *JAMA* **316**, 602–610 (2016).
5. Saran, R. *et al.* US Renal Data System 2018 Annual Data Report: Epidemiology of Kidney Disease in the United States. *Am. J. Kidney Dis.* **73**, A7–A8 (2019).
6. Raja, P. *et al.* The Potential of Albuminuria as a Biomarker of Diabetic Complications. *Cardiovasc. Drugs Ther.* **35**, 455–466 (2021).
7. Papa, C. *et al.* Diabete mellito e ipoglicemie - Nefropatia Diabetica. *Rugarli - Med. interna Sist.* 1671–1673 (2021).
8. Perkins, B. *et al.* In patients with type 1 diabetes and new-onset microalbuminuria the development of advanced chronic kidney disease may not require progression to proteinuria. *Kidney Int.* **77**, 57–64 (2010).
9. Barutta, F. *et al.* The future of diabetic kidney disease management: what to expect from the experimental studies? *J. Nephrol.* **33**, 1151–1161 (2020).
10. Guan, S. S. *et al.* ATP synthase subunit-β down-regulation aggravates diabetic nephropathy. *Sci. Rep.* **5**, 1–15 (2015).
11. Caramori, M. L. *et al.* Renal lesions predict progression of diabetic nephropathy in type 1 diabetes. *J. Am. Soc. Nephrol.* **24**, 1175–1181 (2013).
12. Pagtalunan, M. E. *et al.* Podocyte loss and progressive glomerular injury in type II diabetes. *J. Clin. Invest.* **99**, 342–348 (1997).
13. Marshall, C. B *et al*. Rethinking glomerular basement membrane thickening in diabetic nephropathy: Adaptive or pathogenic? *Am. J. Physiol. - Ren. Physiol.* **311**, F831–F843 (2016).
14. Qian, Y. *et al.* From fibrosis to sclerosis: Mechanisms of glomerulosclerosis in diabetic nephropathy. *Diabetes* **57**, 1439–1445 (2008).
15. Scott, R. P. and Quaggin, S. E. The cell biology of renal filtration. *J. Cell Biol.* **209**, 199–210 (2015).
16. Garg, P. A Review of Podocyte Biology. *Am. J. Nephrol.* **47**, 3–13 (2018).
17. Mundel, P. and Shankland, S. J. Podocyte biology and response to injury. *J. Am. Soc. Nephrol.* **13**, 3005–3015 (2002).
18. Liu, L. *et al.* Defective nephrin trafficking caused by missense mutations in the NPHS1 gene: Insight into the mechanisms of congenital nephrotic syndrome. *Hum. Mol. Genet.* **10**, 2637–2644 (2001).
19. Nagata, M. Podocyte injury and its consequences. *Kidney Int.* **89**, 1221–1230 (2016).

20. Trial, C. Effect of intensive therapy on the development and progression of diabetic nephropathy in the Diabetes Control and Complications Trial. *Kidney Int.* **47**, 1703–1720 (1995).

21. Turner, R. Intensive blood-glucose control with sulphonylureas or insulin compared with conventional treatment and risk of complications in patients with type 2 diabetes (UKPDS 33). *Lancet* **352**, 837–853 (1998).

22. Barr, C. C. Retinopathy and nephropathy in patients with type 1 diabetes four years after a trial of intensive insulin therapy. *Surv. Ophthalmol.* **45**, 459–460 (2001).

23. Li, C. and Siragy, H. M. High glucose induces podocyte injury via enhanced (Pro)renin receptor-Wnt-β-catenin-snail signaling pathway. *PLoS One* **9**, 1–8 (2014).

24. Iglesias-De la Cruz, M. C. *et al.* Effects of high glucose and TGF-β1 on the expression of collagen IV and vascular endothelial growth factor in mouse podocytes. *Kidney Int.* **62**, 901–913 (2002).

25. Gruden, G. *et al.* Insight on the Pathogenesis of Diabetic Nephropathy from the Study of Podocyte and Mesangial Cell Biology. *Curr. Diabetes Rev.* **1**, 27–40 (2005).

26. Brownlee, M. The pathobiology of diabetic complications: A unifying mechanism. *Diabetes* **54**, 1615–1625 (2005).

27. Goh, S. Y. and Cooper, M. E. The role of advanced glycation end products in progression and complications of diabetes. *J. Clin. Endocrinol. Metab.* **93**, 1143–1152 (2008).

28. Forbes, J. M. and Cooper, M. E. Mechanisms of diabetic complications. *Physiol. Rev.* **93**, 137–188 (2013).

29. Riser, B. L. *et al.* Cyclic stretching force selectively up-regulates transforming growth factor-β isoforms in cultured rat mesangial cells. *Am. J. Pathol.* **148**, 1915–1923 (1996).

30. Gruden, G. *et al.* Mechanical stretch-induced fibronectin and transforming growth factor- β1 production in human mesangial cells is p38 mitogen-activated protein kinase-dependent. *Diabetes* **49**, 655–661 (2000).

31. Petermann, A. T. *et al.* Mechanical stress reduces podocyte proliferation in vitro. *Kidney Int.* **61**, 40–50 (2002).

32. Endlich, N. *et al.* Podocytes respond to mechanical stress in vitro. *J. Am. Soc. Nephrol.* **12**, 413–422 (2001).

33. Endlich, N. *et al.* Analysis of differential gene expression in stretched podocytes: osteopontin enhances adaptation of podocytes to mechanical stress. *FASEB J.* **16**, 1850–1852 (2002).

34. Dessapt, C. *et al.* Mechanical forces and TGFβ1 reduce podocyte adhesion through α3β1 integrin downregulation. *Nephrol. Dial. Transplant.* **24**, 2645–2655 (2009).

35. Kliewe, F. *et al.* Studying the role of fascin-1 in mechanically stressed podocytes. *Sci. Rep.* **7**, 1–14 (2017).

36. Jha, J. C. *et al.* Diabetes and Kidney Disease: Role of Oxidative Stress. *Antioxidants Redox Signal.* **25**, 657–684 (2016).

37. Tang, W. H. *et al.* Aldose reductase, oxidative stress, and diabetic mellitus. *Front. Pharmacol.* **3**, 1–8 (2012).

38. Forbes, J. M. *et al.*Oxidative stress as a major culprit in kidney disease in diabetes. *Diabetes* **57**, 1446–1454 (2008).

39. Sifuentes-Franco, S. *et al.* Oxidative stress, apoptosis, and mitochondrial function in diabetic nephropathy. *Int. J. Endocrinol.* **2018**, (2018).

40. Birk, A. V. *et al.* Targeting mitochondrial cardiolipin and the cytochrome c/cardiolipin complex to promote electron transport and optimize mitochondrial ATP synthesis. *Br. J. Pharmacol.* **171**, 2017–2028 (2014).

41. Wan, J. *et al.* Regulation of Respiration and Apoptosis by Cytochrome c Threonine 58 Phosphorylation. *Sci. Rep.* **9**, 1–16 (2019).

42. Zhou, R. *et al.* A role for mitochondria in NLRP3 inflammasome activation. *Nature* **469**, 221–226 (2011).

43. Galvan, D. L. *et al.* Real-time in vivo mitochondrial redox assessment confirms enhanced mitochondrial reactive oxygen species in diabetic nephropathy. *Kidney Int.* **92**, 1282–1287 (2017).

44. Miyamoto, S. *et al.* Restoring mitochondrial superoxide levels with elamipretide (MTP-131) protects db/db mice against progression of diabetic kidney disease. *J. Biol. Chem.* **295**, 7249–7260 (2020).

45. Xiao, L. *et al.* The mitochondria-targeted antioxidant MitoQ ameliorated tubular injury mediated by mitophagy in diabetic kidney disease via Nrf2/PINK1. *Redox Biol.* **11**, 297–311 (2017).

46. Jha, J. C. *et al.* Genetic targeting or pharmacologic inhibition of NADPH oxidase Nox4 provides renoprotection in long-term diabetic nephropathy. *J. Am. Soc. Nephrol.* **25**, 1237–1254 (2014).

47. Jha, J. C. *et al.* NADPH oxidase Nox5 accelerates renal injury in diabetic nephropathy. *Diabetes* **66**, 2691–2703 (2017).

48. Nam, B. Y. *et al.* The MCP-1/CCR2 axis in podocytes is involved in apoptosis induced by diabetic conditions. *Apoptosis* **17**, 1–13 (2012).

49. Sassy-Prigent, C. *et al.* Early glomerular macrophage recruitment in streptozotocin-induced diabetic rats. *Diabetes* **49**, 466–475 (2000).

50. Nguyen, D. *et al.* Macrophage accumulation in human progressive diabetic nephropathy. *Nephrology* **11**, 226–231 (2006).

51. Chow, F. Y. *et al.* Monocyte chemoattractant protein-1-induced tissue inflammation is critical for the development of renal injury but not type 2 diabetes in obese db/db mice. *Diabetologia* **50**, 471–480 (2007).

52. Chow, F. Y. *et al.* Monocyte chemoattractant protein-1 promotes the development of diabetic renal injury in streptozotocin-treated mice. *Kidney Int.* **69**, 73–80 (2006).

53. You, H., *et al.* Macrophages directly mediate diabetic renal injury. *Am. J. Physiol. - Ren. Physiol.* **305**, 1719–1727 (2013).

54. Pawluczyk, I. Z. A. and Harris, K. P. G. Macrophages promote prosclerotic responses in cultured rat mesangial cells: A mechanism for the initiation of glomerulosclerosis. *J. Am. Soc. Nephrol.* **8**, 1525–1536 (1997).

55. Ikezumi, Y. *et al.* Activated macrophages down-regulate podocyte nephrin and podocin expression via stress-activated protein kinases. *Biochem. Biophys. Res. Commun.* **376**, 706–711 (2008).

56. Kanamori, H. *et al.* Inhibition of MCP-1/CCR2 pathway ameliorates the development of diabetic nephropathy. *Biochem. Biophys. Res. Commun.* **360**, 772–777 (2007).

57. Saxena, S., *et al.* Critical role of mitochondrial dysfunction and impaired mitophagy in diabetic nephropathy. *J. Cell. Physiol.* **234**, 19223–19236 (2019).

58. Imasawa, T. *et al.* High glucose repatterns human podocyte energy metabolism during differentiation and diabetic nephropathy. *FASEB J.* **31**, 294–307 (2017).

59. Ducasa, G. M. *et al.* ATP-binding cassette A1 deficiency causes cardiolipin-driven mitochondrial dysfunction in podocytes. *J. Clin. Invest.* **129**, 3387–3400 (2019).

60. Li, J. *et al.* Smad4 promotes diabetic nephropathy by modulating glycolysis and OXPHOS . *EMBO Rep.* **21**, 1–20 (2020).

61. Arciuch, V. G. A. *et al.* Mitochondrial regulation of cell cycle and proliferation. *Antioxidants Redox Signal.* **16**, 1150–1180 (2012).

62. Hamanaka, R. B. and Chandel, N. S. Mitochondrial reactive oxygen species regulate cellular signaling and dictate biological outcomes. *Trends Biochem. Sci.* **35**, 505–513 (2010).

63. Su, Y. J. *et al.* Increasing high-sensitive C-reactive protein level predicts peritonitis risk in chronic peritoneal dialysis patients. *BMC Nephrol.* **14**, (2013).

64. Tin, A. *et al.* Association between mitochondrial DNA copy number in peripheral blood and incident CKD in the atherosclerosis risk in communities study. *J. Am. Soc. Nephrol.* **27**, 2467–2473 (2016).

65. Audzeyenka, I. *et al.* Hyperglycemia alters mitochondrial respiration efficiency and mitophagy in human podocytes. *Exp. Cell Res.* **407**, 112758 (2021).

66. Wai, T. and Langer, T. Mitochondrial Dynamics and Metabolic Regulation. *Trends Endocrinol. Metab.* **27**, 105–117 (2016).

67. Burman, J. L. *et al.* Mitochondrial fission facilitates the selective mitophagy of protein aggregates. *J. Cell Biol.* **216**, 3231–3247 (2017).

68. Ventura-Clapier, R., *et al.* Transcriptional control of mitochondrial biogenesis: The central role of PGC-1α. *Cardiovasc. Res.* **79**, 208–217 (2008).

69. Xiao, L. *et al.* Rap1 ameliorates renal tubular injury in diabetic nephropathy. *Diabetes* **63**, 1366–1380 (2014).

70. Zhan, M., *et al.* Disruption of Renal Tubular Mitochondrial Quality Control by Myo-Inositol Oxygenase in Diabetic Kidney Disease. *J. Am. Soc. Nephrol.* **26**, 1304–1321 (2015).

71. Ayanga, B. A. *et al.* Dynamin-related protein 1 deficiency improves mitochondrial fitness and protects against progression of diabetic nephropathy. *J. Am. Soc. Nephrol.* **27**, 2733–2747 (2016).

72. McLelland, G. L., *et al.* Parkin and PINK1 function in a vesicular trafficking pathway regulating mitochondrial quality control. *EMBO J.* **33**, 282–295 (2014).

73. Li, W. *et al.* Effects of overexpressing FoxO1 on apoptosis in glomeruli of diabetic mice and

in podocytes cultured in high glucose medium. *Biochem. Biophys. Res. Commun.* **478**, 612–617 (2016).

74. Sun, J. *et al.* CoQ10 ameliorates mitochondrial dysfunction in diabetic nephropathy through mitophagy. *J. Endocrinol.* **240**, 445–465 (2019).

75. Li, W. *et al.* FoxO1 promotes mitophagy in the podocytes of diabetic male mice via the PINK1/parkin pathway. *Endocrinology* **158**, 2155–2167 (2017).

76. Sharma, K. *et al.* Metabolomics reveals signature of mitochondrial dysfunction in diabetic kidney disease. *J. Am. Soc. Nephrol.* **24**, 1901–1912 (2013).

77. Li, S. Y. *et al.* Increasing the level of peroxisome proliferator-activated receptor γ coactivator-1α in podocytes results in collapsing glomerulopathy. *JCI insight* **2**, (2017).

78. Rustom, A. The missing link: Does tunnelling nanotube-based supercellularity provide a new understanding of chronic and lifestyle diseases? *Open Biol.* **6**, (2016).

79. Rustom, A. *et al.* Nanotubular Highways for Intercellular Organelle Transport. *Science (80-.).* **303**, 1007–1010 (2004).

80. Hase, K. *et al.* M-Sec promotes membrane nanotube formation by interacting with Ral and the exocyst complex. *Nat. Cell Biol.* **11**, 1427–1432 (2009).

81. Eugenin, E. A. *et al.* Tunneling nanotubes (TNT) are induced by HIV-infection of macrophages: A potential mechanism for intercellular HIV trafficking. *Cell. Immunol.* **254**, 142–148 (2009).

82. Watkins, S. C. and Salter, R. D. Functional connectivity between immune cells mediated by tunneling nanotubules. *Immunity* **23**, 309–318 (2005).

83. Salter, R. D. and Watkins, S. C. Dynamic Properties of Antigen Between Dendritic Cells. *Immunol. Res.* 211–220 (2006).

84. Xu, W. *et al.* HIV-1 evades virus-specific IgG2 and IgA responses by targeting systemic and intestinal B cells via long-range intercellular conduits. *Nat. Immunol.* **10**, 1008–1017 (2009).

85. Galkina, S. I. *et al.* Microbial alkaloid staurosporine induces formation of nanometer-wide membrane tubular extensions (cytonemes, membrane tethers) in human neutrophils. *Cell Adhes. Migr.* **4**, 32–38 (2010).

86. Yasuda, K. *et al.* Adriamycin nephropathy: A failure of endothelial progenitor cell-induced repair. *Am. J. Pathol.* **176**, 1685–1695 (2010).

87. Roehlecke, C. and Schmidt, M. H. H. Tunneling nanotubes and tumor microtubes in cancer. *Cancers (Basel).* **12**, 1–21 (2020).

88. Mittal, R. *et al.* Cell communication by tunneling nanotubes: Implications in disease and therapeutic applications. *J. Cell. Physiol.* **234**, 1130–1146 (2019).

89. Chinnery, H. R., *et al.* Cutting Edge: Membrane Nanotubes In Vivo: A Feature of MHC Class II + Cells in the Mouse Cornea . *J. Immunol.* **180**, 5779–5783 (2008).

90. Seyed-Razavi, Y. *et al.*Membrane nanotubes in myeloid cells in the adult mouse cornea represent a novel mode of immune cell interaction. *Immunol. Cell Biol.* **91**, 89–95 (2013).

91. Parker, I. *et al.* Lattice light sheet imaging of membrane nanotubes between human breast cancer cells in culture and in brain metastases. *Sci. Rep.* **7**, 1–7 (2017).

92. Weil, S. *et al.* Tumor microtubes convey resistance to surgical lesions and chemotherapy in gliomas. *Neuro. Oncol.* **19**, 1316–1326 (2017).

93. Alarcon-Martinez, L. *et al.* Interpericyte tunnelling nanotubes regulate neurovascular coupling. *Nature* **585**, 91–95 (2020).

94. Desir, S. *et al.* Chemotherapy-Induced Tunneling Nanotubes Mediate Intercellular Drug Efflux in Pancreatic Cancer. *Sci. Rep.* **8**, 1–13 (2018).

95. Osswald, M. *et al.* Brain tumour cells interconnect to a functional and resistant network. *Nature* **528**, 93–98 (2015).

96. Wolft, F. W. *et al.* B94 , a Primary Response Gene Inducible by Tumor Necrosis Factor-a , Is Expressed in Developing Hematopoietic Tissues and the Sperm Acrosome *. *J. Biol. Chem.* **269**, 3633–3640 (1994).

97. Ranzinger, J. *et al.* Nanotube action between human mesothelial cells reveals novel aspects of inflammatory responses. *PLoS One* **6**, (2011).

98. Ohno, H. *et al.* M-sec emerging secrets of TNT formation Ohno 2010. 231–233 (2010) doi:10.1038/ncb1990.unneling.

99. Burridge, K. and Wennerberg, K. Rho and Rac Take Center Stage. *Cell* **116**, 167–179 (2004).

100. Ohta, Y. *et al.*The small GTPase RaIA targets filamin to induce filopodia. *Proc. Natl. Acad. Sci. U. S. A.* **96**, 2122–2128 (1999).

101. Sugihara, K. *et al.* The exocyst complex binds the small GTPase RalA to mediate filopodia formation. *Nat. Cell Biol.* **4**, 73–78 (2002).

102. Zhang, Y. Tunneling-nanotube. *Commun. Integr. Biol.* **4**, 324–325 (2011).

103. Takahashi, A. *et al.* Tunneling nanotube formation is essential for the regulation of osteoclastogenesis. *J. Cell. Biochem.* **114**, 1238–1247 (2013).

104. Wang, X., Bukoreshtliev, N. V. & Gerdes, H. H. Developing Neurons Form Transient Nanotubes Facilitating Electrical Coupling and Calcium Signaling with Distant Astrocytes. *PLoS One* **7**, 1–9 (2012).

105. Gerdes, H. H. *et al.*Tunneling nanotubes, an emerging intercellular communication route in development. *Mech. Dev.* **130**, 381–387 (2013).

106. Sun, X. *et al.* Tunneling-nanotube direction determination in neurons and astrocytes. *Cell Death Dis.* **3**, (2012).

107. Sheng, Z. H. and Cai, Q. Mitochondrial transport in neurons: Impact on synaptic homeostasis and neurodegeneration. *Nat. Rev. Neurosci.* **13**, 77–93 (2012).

108. Islam, M. N. *et al.* Mitochondrial transfer from bone-marrow-derived stromal cells to pulmonary alveoli protects against acute lung injury. *Nat. Med.* **18**, 759–765 (2012).

109. Li, X. *et al.* Mitochondrial transfer of induced pluripotent stem cell-derived mesenchymal stem cells to airway epithelial cells attenuates cigarette smoke-induced damage. *Am. J. Respir. Cell Mol. Biol.* **51**, 455–465 (2014).

110. Qin, Y. *et al.* The Functions, Methods, and Mobility of Mitochondrial Transfer Between Cells. *Front. Oncol.* **11**, 1–14 (2021).

111. Plotnikov, E. Y. *et al.*Cytoplasm and organelle transfer between mesenchymal multipotent stromal cells and renal tubular cells in co-culture. *Exp. Cell Res.* **316**, 2447–2455 (2010).

112. Hayakawa, K. *et al.* Transfer of mitochondria from astrocytes to neurons after stroke. *Nature* **535**, 551–555 (2016).

113. Feng, Y. *et al.* Human Bone Marrow Mesenchymal Stem Cells Rescue Endothelial Cells Experiencing Chemotherapy Stress by Mitochondrial Transfer Via Tunneling Nanotubes. *Stem Cells Dev.* **28**, 674–682 (2019).

114. Wang, X. *et al.* Rescue of Brain Function Using Tunneling Nanotubes Between Neural Stem Cells and Brain Microvascular Endothelial Cells. *Mol. Neurobiol.* **53**, 2480–2488 (2016).

115. Babenko, V. A. *et al.* Miro1 enhances mitochondria transfer from multipotent mesenchymal stem cells (MMSC) to neural cells and improves the efficacy of cell recovery. *Molecules* **23**, 1–14 (2018).

116. Önfelt, B. *et al.* M. Cutting Edge: Membrane Nanotubes Connect Immune Cells. *J. Immunol.* **173**, 1511–1513 (2004).

117. Vallabhaneni, K. C. *et al.* Vascular smooth muscle cells initiate proliferation of mesenchymal stem cells by mitochondrial transfer via tunneling nanotubes. *Stem Cells Dev.* **21**, 3104–3113 (2012).

118. Acquistapace, A. *et al.* Human mesenchymal stem cells reprogram adult cardiomyocytes toward a progenitor-like state through partial cell fusion and mitochondria transfer. *Stem Cells* **29**, 812–824 (2011).

119. Hashimoto, M. *et al.* Potential Role of the Formation of Tunneling Nanotubes in HIV-1 Spread in Macrophages. *J. Immunol.* **196**, 1832–1841 (2016).

120. Panasiuk, M. *et al.* Tunneling Nanotubes as a Novel Route of Cell-to-Cell Spread of Herpesviruses. *J. Virol.* **92**, (2018).

121. Aguzzi, A. and Lakkaraju, A. K. K. Cell Biology of Prions and Prionoids: A Status Report. *Trends Cell Biol.* **26**, 40–51 (2016).

122. Wang, J. *et al.* Cell adhesion-mediated mitochondria transfer contributes to mesenchymal stem cell-induced chemoresistance on T cell acute lymphoblastic leukemia cells. *J. Hematol. Oncol.* **11**, 1–13 (2018).

123. Barutta, F. *et al.* Protective role of the M-sec-tunneling nanotube system in podocytes. *J. Am. Soc. Nephrol.* **32**, 1114–1130 (2021).

124. Almalki, S. G. and Agrawal, D. K. Key transcription factors in the differentiation of mesenchymal stem cells. *Differentiation* **92**, 41–51 (2016).

125. Feng-Juan LV. *et al.* Concise Review: The Surface Markers and Identity of Human Mesenchymal Stem Cell. *Stem Cells* **32**, 1408–1419 (2014).

126. Mushahary, D. *et al.* Isolation, cultivation, and characterization of human mesenchymal stem cells. *Cytom. Part A* **93**, 19–31 (2018).

127. Fukuchi, Y. *et al.* Human Placenta-Derived Cells Have Mesenchymal Stem/Progenitor Cell Potential. *Stem Cells* **22**, 649–658 (2004).

128. Baksh, D. *et al.* Comparison of Proliferative and Multilineage Differentiation Potential of Human Mesenchymal Stem Cells Derived from Umbilical Cord and Bone Marrow. *Stem*

Cells **25**, 1384–1392 (2007).

129. Eirin, A. *et al.* Adipose tissue-derived mesenchymal stem cells improve revascularization outcomes to restore renal function in swine atherosclerotic renal artery stenosis. *Stem Cells* **30**, 1030–1041 (2012).

130. Wang, S. *et al.* Mesenchymal Stem Cells Ameliorate Podocyte Injury and Proteinuria in a Type 1 Diabetic Nephropathy Rat Model. *Biol. Blood Marrow Transplant.* **19**, 538–546 (2013).

131. Lv, S. S. *et al.* Mesenchymal stem cells transplantation ameliorates glomerular injury in streptozotocin-induced diabetic nephropathy in rats via inhibiting macrophage infiltration. *Int. Immunopharmacol.* **17**, 275–282 (2013).

132. Yuan, Y. *et al.* Mesenchymal stem cells elicit macrophages into M2 phenotype via improving transcription factor EB-mediated autophagy to alleviate diabetic nephropathy. *Stem Cells* **38**, 639–652 (2020).

133. Ezquer, F. *et al.* Proregenerative microenvironment triggered by donor mesenchymal stem cells preserves renal function and structure in mice with severe diabetes mellitus. *Biomed Res. Int.* **2015**, (2015).

134. Nagaishi, K. *et al.* Mesenchymal stem cell therapy ameliorates diabetic nephropathy via the paracrine effect of renal trophic factors including exosomes. *Sci. Rep.* **6**, 1–16 (2016).

135. Li, H. *et al.* Paracrine effect of mesenchymal stem cell as a novel therapeutic strategy for diabetic nephropathy. *Life Sci.* **215**, 113–118 (2018).

136. Ebrahim, N. *et al.* Mesenchymal Stem Cell-Derived Exosomes Ameliorated Diabetic Nephropathy by Autophagy Induction through the mTOR Signaling Pathway. *Cells* **7**, 226 (2018).

137. Grange, C. *et al.* Stem cell-derived extracellular vesicles inhibit and revert fibrosis progression in a mouse model of diabetic nephropathy. *Sci. Rep.* **9**, 1–13 (2019).

138. Ahmad, T. *et al.* Miro1 regulates intercellular mitochondrial transport & enhances mesenchymal stem cell rescue efficacy. *EMBO J.* **33**, 994–1010 (2014).

139. Las, G. and Shirihai, O. S. Miro1: New wheels for transferring mitochondria. *EMBO J.* **33**, 939–941 (2014).

140. Liu, K. *et al.* Mesenchymal stem cells rescue injured endothelial cells in an in vitro ischemia-reperfusion model via tunneling nanotube like structure-mediated mitochondrial transfer. *Microvasc. Res.* **92**, 10–18 (2014).

141. Han, H. *et al.* Bone marrow-derived mesenchymal stem cells rescue injured H9c2 cells via transferring intact mitochondria through tunneling nanotubes in an in vitro simulated ischemia/reperfusion model. *Mol. Med. Rep.* **13**, 1517–1524 (2016).

142. Jiang, D. *et al.* Mitochondrial transfer of mesenchymal stem cells effectively protects corneal epithelial cells from mitochondrial damage. *Cell Death Dis.* **7**, e2467-10 (2016).

143. Plotnikov, E. Y. *et al.* Cell-to-cell cross-talk between mesenchymal stem cells and cardiomyocytes in co-culture. *J. Cell. Mol. Med.* **12**, 1622–1631 (2008).

144. Yang, H. *et al.* Biochip-based study of unidirectional mitochondrial transfer from stem cells to myocytes via tunneling nanotubes. *Biofabrication* **8**, 15012 (2016).

145. Jackson, M. V. *et al.* Mitochondrial Transfer via Tunneling Nanotubes is an Important Mechanism by Which Mesenchymal Stem Cells Enhance Macrophage Phagocytosis in the In Vitro and In Vivo Models of ARDS. *Stem Cells* **34**, 2210–2223 (2016).

146. Delage, E. *et al.* Differential identity of Filopodia and Tunneling Nanotubes revealed by the opposite functions of actin regulatory complexes. *Sci. Rep.* **6**, 25–28 (2016).

147. Whitehead, J. *et al.* Tunneling nanotubes mediate the expression of senescence markers in mesenchymal stem/stromal cell spheroids. *Stem Cells* **38**, 80–89 (2020).

148. Gabriel, S. S. *et al.* Bone marrow transplantation improves proximal tubule dysfunction in a mouse model of Dent disease. *Kidney Int.* **91**, 842–855 (2017).

149. Thayanithy, V. *et al.* Tumor-stromal cross talk: Direct cell-to-cell transfer of oncogenic microRNAs via tunneling nanotubes. *Transl. Res.* **164**, 359–365 (2014).

150. Lou, E. *et al.* Tunneling nanotubes provide a unique conduit for intercellular transfer of cellular contents in human malignant pleural mesothelioma. *PLoS One* **7**, 1–11 (2012).

151. Schiller, C. *et al.* LST1 promotes the assembly of a molecular machinery responsible for tunneling nanotube formation. *J. Cell Sci.* **126**, 767–777 (2013).

152. Zhang, Y. *et al.* iPSC-MSCs with High Intrinsic MIRO1 and Sensitivity to TNF-α Yield Efficacious Mitochondrial Transfer to Rescue Anthracycline-Induced Cardiomyopathy. *Stem Cell Reports* **7**, 749–763 (2016).

153. Torralba, D. *et al.* Mitochondria know no boundaries: Mechanisms and functions of intercellular mitochondrial transfer. *Front. Cell Dev. Biol.* **4**, 1–11 (2016).

154. Konari, N. *et al.* Mitochondria transfer from mesenchymal stem cells structurally and functionally repairs renal proximal tubular epithelial cells in diabetic nephropathy in vivo. *Sci. Rep.* **9**, (2019).

155. Patrakka, J. and Tryggvason, K. New insights into the role of podocytes in proteinuria. *Nat. Rev. Nephrol.* **5**, 463–468 (2009).

156. Doublier, S. *et al.* Nephrin expression is reduced in human diabetic nephropathy: Evidence for a distinct role for glycated albumin and angiotensin II. *Diabetes* **52**, 1023–1030 (2003).

157. Wharram, B. L. Podocyte Depletion Causes Glomerulosclerosis: Diphtheria Toxin-Induced Podocyte Depletion in Rats Expressing Human Diphtheria Toxin Receptor Transgene. *J. Am. Soc. Nephrol.* **16**, 2941–2952 (2005).

158. Zhang, W. *et al.* Neural stem cell transplantation enhances mitochondrial biogenesis in a transgenic mouse model of Alzheimer's disease-like pathology. *Neurobiol. Aging* **36**, 1282–1292 (2015).

159. Szeto, H. H. *et al.* Protection of mitochondria prevents high-fat diet–induced glomerulopathy and proximal tubular injury. *Kidney Int.* **90**, 997–1011 (2016).

160. Saito, Y. *et al.* Suppression of nephrin expression by TNF-α via interfering with the cAMP-retinoic acid receptor pathway. *Am. J. Physiol. - Ren. Physiol.* **298**, 1436–1444 (2010).